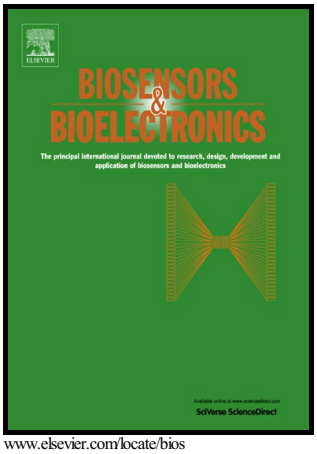

www.elsevier.com/locate/bios

Versatile Graphene Biosensors for Enhancing Human Cell Therapy

George M. Vlăsceanu, Roxana-Maria Amărandi, Mariana Ioniță, Teddy Tite, Horia Iovu, Luisa Pilan, Jorge S. Burns

PII: S0956-5663(18)30321-X
DOI: https://doi.org/10.1016/j.bios.2018.04.053
Reference: BIOS10449

To appear in: *Biosensors and Bioelectronic*

Received date: 13 February 2018
Revised date: 18 April 2018
Accepted date: 25 April 2018

Cite this article as: George M. Vlăsceanu, Roxana-Maria Amărandi, Mariana Ioniță, Teddy Tite, Horia Iovu, Luisa Pilan and Jorge S. Burns, Versatile Graphene Biosensors for Enhancing Human Cell Therapy, *Biosensors and Bioelectronic,* https://doi.org/10.1016/j.bios.2018.04.053

Versatile Graphene Biosensors for Enhancing Human Cell Therapy

George M. Vlăsceanu[a,b], Roxana-Maria Amărandi[b], Mariana Ioniță[a,b], Teddy Tite[b], Horia Iovu[a,d], Luisa Pilan[*c] and Jorge S. Burns[*b]

[a]Advanced Polymer Materials Group, University Politehnica of Bucharest, Gh Polizu 1-7, 011061, Bucharest, Romania
[b]Faculty of Medical Engineering, University Politehnica of Bucharest, Gh Polizu 1-7, 011061, Bucharest, Romania
[c]Department of Inorganic Chemistry, Physical Chemistry and Electrochemistry, University Politehnica of Bucharest, 1-7, Polizu St., Bucharest, Romania
[d]Academy of Romanian Scientists, Splaiul Independentei 107, Bucharest, Romania

*Corresponding authors

jsburns@unimore.it
luisa_pilan@yahoo.com

Abstract

Technological advances in engineering and cell biology stimulate novel approaches for medical treatment, in particular cell-based therapy. The first cell-based gene therapy against cancer was recently approved by the US Food and Drug Administration. Progress in cancer diagnosis includes a blood test detecting five cancer types. Numerous stem cell phase I/II clinical trials showing safety and efficacy will soon pursue qualifying criteria for advanced therapy medicinal products (ATMP), aspiring to join the first stem-cell therapy approved by the European Medicines Agency. Cell based therapy requires extensive preclinical characterisation of biomarkers indicating mechanisms of action crucial to the desired therapeutic effect. Quantitative assays monitoring critical functions for the manufacture of optimal cell and tissue-based clinical products, include successful potency assays for implementation. The challenge to achieve high quality measurement is increasingly met by progress in biosensor design. We adopt a cell therapy perspective to highlight recent examples of graphene-enhanced biointerfaces for measurement of biomarkers relevant to cancer treatment, diagnosis and tissue regeneration. Graphene based biosensor design problems can thwart their use for health care transformative point of care testing and real-time applications. We discuss concerns to be addressed and emerging solutions for establishing clinical grade biosensors to accelerate human cell therapy.

Keywords

Biosensors
Graphene
Cancer
Cell Therapy
Stem cells
Theranostics

1. Introduction

Cell based therapeutics have been described as the next pillar of medicine (Fischbach et al., 2013) expanding synthetic small-molecule drugs and biologics. Advantages of complex sensing and response systems, directed cell migration, autoregulation and more precise dynamic control over levels and duration of action, have placed cell therapy at the forefront of new interventions for hard-to-treat cancers and regenerative medicine. The associated cell expansion industry requires broad collaboration and systems engineering approaches to meet the demands of clinical scale application. Supporting two-dimensional (2D) and three-dimensional (3D) cell culture approaches are innovative growth factors, biomaterials and bioreactors (McKee & Chaudhry, 2017) and advanced technologies such as 3D printing (Maartens et al., 2017). Concurrent advances in the nanoscale

material sciences now drive convergence of highly augmented multidisciplinary research. Supramolecular chemistry, preparing materials from small-molecule precursors in a modular fashion, broadens the scope of biomaterials applicable to anti-cancer drug delivery, tissue engineering, regenerative medicine, immunology (Webber et al., 2016) and biosensor design (Bollella et al., 2017).

A cell-based therapeutic needs close monitoring of an integrated and efficient product work-flow. Rigorous guidelines for cell based therapy counteract the problem of unproven cell therapies by stipulating identity, purity, safety and potency as critical quality attributes (CQA) of Cell Based Medical Products (CBMP) within the classification of Advanced Therapy Medical Product (ATMP). Autologous cell treatment approaches usually need cell expansion under current good manufacturing practice (cGMP) culture conditions to accrue a minimal therapeutic cell dose before prompt administration (Gómez-Barrena et al., 2015). Manufacturing conditions between diverse centers have yet to be fully standardized for cell products to be of equivalent quality and function (Liu et al., 2017), yet will inevitably involve measurement time constraints. Important potency assay criteria address the overall quality, sustainability and desired function of the cell product. Such assays typically adopt surrogate biomarkers for gene expression microarray profiles, flow cytometric analysis, cell cloning, and/or quantitative polymerase chain reaction (PCR)-based methods and there is potential for graphene based biosensors to more conveniently monitor cell product quality (Amărandi et al., 2018).

Biosensors offer a promising solution for improved standards of automated measurement, tailored to a broad range of cell-derived biomarker analytes, including nucleic acids and proteins that may be compartmentalised as nuclear, cytoplasmic, cell surface or secreted. Rapid analysis from minimal amounts of material allows adaptation to prompt workflows with an additional advantage that integrated design platforms can be suitable for clinical point-of care (POC) measurement (Syedmoradi et al., 2017). Intrinsic properties of graphene have rendered it a material of choice for biosensor development, especially given many functionalization options for incorporation in nanobiocomposites (Ioniţă et al., 2017). Thus graphene based biosensors can support a range of specific biological receptors whilst maintaining ultrasensitive transducer qualities for efficient measurement (Suvarnaphaet & Pechprasarn, 2017). Intrinsic qualities of graphene favour versatility. Excellent conductivity of electrical charge and high surface to volume ratio are well suited for electrochemical biosensors whilst long-range nanoscale resonance energy transfer properties confer broad-spectrum organic dye quenching capabilities for optical sensors (Ma et al., 2013).

2. The aptness of graphene-based biosensors

Within complex cell culture or tissue isolates, detection of a characteristic functional biomarker requires powerful signal transduction of the biorecognition event (Patil et al., 2015). Graphene's honeycomb lattice sheet of sp^2-bonded carbon atoms has exceptional experimentally confirmed mechanical strength (Uder et al., 2018). Electron transfer ability and excellent thermal conductivity is nonetheless influenced by defect density (Malekpour et al., 2016), requiring delicate control of geometric and electronic structure. Outcomes of diversely explored preparation methods include single or few layer graphene, graphene oxide (GO) and chemically, electrochemically or thermally reduced graphene oxide (rGO), that can be further decorated or functionalized by covalent or noncovalent methods to manufacture composites. Nanographene forms, with at least one dimension between 1 and 100 nm, include graphene nanoribbons (GNR) and graphene quantum dots (GQD) (Suvarnaphaet & Pechprasarn, 2017). How to achieve large-scale production processes, is a topic of intense research focus.

Upscaled production by chemical exfoliation methods is becoming feasible, generating few-layer and functionalized forms that retain helpful unique properties (Wang et al., 2017c).

Among the different forms, GO is favoured for biocompatibility and biodegradability, dispersivity in aqueous medium and a high specific surface area (≈890 m^2/g) (Montes-Navajas et al., 2013) that can be readily functionalized to accommodate highly active probes in novel biosensor bio-interfaces (Muazim &Hussain, 2017). A broad-spectrum fluorescence quenching ability and room-temperature electron mobility can provide high sensitivity and a wide dynamic range (Janegitz et al., 2017). The performance of the sensors are largely determined by the quality of the graphene film (Liu et al., 2015a). Ultimately, the specific graphene material chosen reflects the target and sensing mechanism, balancing consideration of detection performance, reproducibility, cost, and manufacturability (Liu et al., 2012). GO presents a complementing versatile surface chemistry, compatible with a broad range of biologically relevant sensor materials. Good nucleic acid adsorption properties, facilitates incorporation of aptamers tailored to specifically capture desired analyte targets. Although it is too soon to propose a "best preparation method", attractive approaches include energy efficient and environmentally friendly water electrolytic oxidation of graphite, yielding electrochemically synthesized graphene oxide (EGO). The method was fast and could adaptably control the extent of graphene oxidation and number of layers to tune the EGO properties (Pei et al., 2018).

Compared to materials such as carboxymethylated dextran on the surface of a commercial sensor chip, GO provided three-fold higher sensitivity with 25-fold better non-specific binding properties when used as a biomolecule adsorption substrate in a surface plasmon resonance (SPR) biosensor (Stebunov et al., 2015). GO can be applied as a thin film to various sensor surfaces to not only anchor aptamers but also support cell growth suitable for live-cell biosensing (Foroutan et al., 2017; Ricci et al., 2017; Shin et al., 2017). Unique electronic properties of a graphene layer confer a significantly larger absorption of s-polarization than p-polarization. High-performance refractive index microscopy can monitor reflected intensity variations of s- and p- polarizations simultaneously to achieve both high refractive index sensitivity and longitudinal detection that can penetrate whole cells. Combining cylindrical vector beam common-path focusing with a differential detecting graphene biosensor improved visualization and enhanced real-time monitoring of subcellular dynamic activities (Sun et al., 2018). Notably, cells grown on GO nanosheets showed enhanced membrane ruffling and shedding; non-lethal effects that nonetheless suggest that graphene could influence cellular mechanosensing (Sun et al., 2016a). Although in vitro co-seeding substrate-unattached cells with GO was toxic (Wei et al., 2017), when used as a composite to enrich a 3D chitosan (CHT) scaffold, GO promoted bone formation in a CHT/GO filled murine critical-size calvarial defect model (Hermenean et al., 2017).

Thus graphene and its derivatives can act as a thin veil that bridges how a molecule is sensed and how the sensor is functionalized and passivated to achieve low power high signal-to-noise readouts (Mulvaney et al., 2014). They provide qualities highly suited for a versatile range of biosensors for biomarker analytes (Table 1).

3. Towards cancer theranostics and regenerative medicine

Graphene materials used in biosensing initially succeeded with electrochemical detection of neurotransmitter levels (Shang et al., 2008) and DNA (Mohanty & Berry, 2008). Now adopted for many other applications (Chauhan et al., 2017; Justino et al., 2017), the scope of chemical and biological analytes includes proteins (Mao

et al., 2013), nucleic acids (Zhao et al., 2016), small molecules (Wang et al., 2015a), hazardous dyes (Wang et al., 2014) and even entire bacterial populations (Lian et al., 2015). Here we focus on graphene-based biosensors directed towards use in cell-based biomedicine concerning cancer detection and intervention (Bianying et al., 2013; Cruz et al., 2016; Zhang et al., 2014a; Zhou et al., 2017; Zhu et al., 2016a), and stem cell tissue regeneration (Akhavan, 2016; Bressan et al., 2014; Kim et al., 2015; Menaa et al., 2015; Pryzhkova, 2013).

Early stage cancer diagnosis can be decisive for treatment. Early localized resection is potentially curative if performed before systemic spread of metastases to distant sites. Impressive exploration of tumour-specific biomarker biology has recently introduced a blood test detecting five cancer types with 99% specificity and sensitivity ranging from 69 to 89%. Admittedly, sensitivity would be more rigorously challenged when seeking to detect subclinical earlier stage cancer in a patient cohort of unknown cancer status (Cohen et al., 2018). Graphene-based biosensors are particularly useful for exploring sensitive detection platforms for low abundance biomarker detection (Bollella et al., 2017; Janegitz et al., 2017; Jayanthi et al., 2017). Femtomolar cancer biomarker detection of folic acid proteins was readily achieved using a graphene-coated surface plasmon resonance (SPR) chip interface (He et al., 2017). Relevant to blood tests, an optical rGO-based fluorescent aptasensor was able to detect 1 pM levels of an antibiotic in the complex samples of spiked whole blood, serum or milk (Ha et al., 2017).

Many biomarkers emerging from tumour microenvironment studies analyse fundamental phenotypic traits, each a major topic of research in its own right. In particular, proliferation, senescence, apoptosis, angiogenesis, immunity and autophagy are of fundamental importance not only for tumour biology, but also for stem cell biology and regenerative medicine. Physiological biomarkers influencing these key processes have been utilised in carbon nanomaterial-based biosensors (Fig. 1). Recent biosensor examples highlight that graphene is well suited to theranostic platforms that combine therapy and diagnosis (Muazim & Hussain, 2017).

3.1 Graphene biosensors for miRNA and proliferation

Discovered in 1993, microRNAs (miRNAs) regulate gene expression by post-transcriptionally influencing their target mRNAs and are protagonists in several types of cancer (Drusco & Croce, 2017). Research is revealing an increased functional versatility for these small non-coding RNAs of 20-24 nucleotides, yet a prevalent view is that they often suppress expression of a considerable number of target genes by recognizing complementary target sites of the 3' untranslated region (3'-UTR) of mRNAs (Catalanotto et al., 2016). For cancer diagnosis and stem cell growth monitoring purposes it is convenient that miRNA can also be found in cell-secreted extracellular vesicles (Kinoshita et al., 2017).

In particular, miR-21 modulates the expression of a plethora of genes influencing cell proliferation, including the tumour suppressor genes phosphatase and tensin homologue (PTEN) and programmed cell death 4 (PDCD4) (Buscaglia & Li, 2011; Meng et al., 2007) plus B-cell lymphoma 2 (BCL2) (Chan et al., 2005). Thus, miR-21 could both increase proliferation and decrease apoptosis in cancer cells. Desire for miR-21 quantification has spawned several graphene-based biosensors with a range of detection limits (Cui et al., 2012; Dong et al., 2012; Ryoo et al., 2013; Yin et al., 2012). A magnetic nanoparticle-based Faraday cage-type electrochemiluminescence biosensor adopted multi-functionalized GO as a signalling unit that successfully detected miR-21 in human serum at concentrations as low as 0.3 fM (Lu et al., 2017). However, the authors did not detect endogenous miR-21, but synthetically added miR-21 to blank human serum to show applicability for

biomarker quantification in complex samples. A similar bioassay strategy applied by Azimzadeh et al., quantified another cancer biomarker, miR-155, with the help of a graphene-oxide/gold nanorod (GO/GNR)-modified glassy carbon electrode (GCE) (Azimzadeh et al., 2016). Remarkably, GO/GNR assemblies detected miR-21 at concentrations as low as 0.03 amol/ng of total RNA (Ma et al., 2017). Graphene-biocomposite biosensors can combine functions as imaging agents and therapeutic effectors. For example, a hyaluronic acid-conjugated graphene oxide (HA-GO) nanoplatform performed simultaneous in vivo detection of miR-21 and its inhibition (Hwang et al., 2017). The HA-GO composite, helped direct nanoplatform uptake via endocytosis mediated by the high-affinity surface antigen CD44, abundant in cancer cells (Senbanjo & Chellaiah, 2017). The bimodal nanoplatform used a GO quenched fluorescently labelled complementary probe to detect miR-21 and specific hybridization-mediated sequestration that down-regulated miR-21 bioactivity and inhibited tumour progression. In a recent study, aptamer-conjugated porphyrin-modified PEGylated graphene quantum dots theranostically detected cancer-associated miRNAs and delivered photothermal/photodynamic synergetic therapy that effectively reduced experimentally-induced tumours by 86% (Cao et al., 2017b).

3.2 Biosensing cell senescence

The p53 tumour suppressor gene product tumour protein 53 (TP53) is networked to regulate cancer cell proliferation, apoptosis and senescence (Reinhardt &Schumacher, 2012). With also roles in stem cell self-renewal, differentiation and reprogramming (Spike &Wahl, 2011), TP53 can claim centre stage as a biosensor target and featured prominently in the CancerSEEK blood test (Cohen et al., 2018). Subject to gene mutations and epigenetic modifications, its DNA sequence, mRNA expression and protein levels are all relevant to interpreting its role. A disposable reduced graphene oxide-carboxymethylcellulose-modified screen-printed carbon electrode (rGO-CMC-modified SPCE) electrochemically characterised the p53 gene sequence with a 3 nM detection limit, discriminating single nucleotide polymorphisms in specific cancer cell lines (Esteban-Fernández de Ávila et al., 2015). Alternatively, TP53 protein was sensitively quantified in normal and cancer cell lines using a biofuel-cell-based self-powered biosensor containing a DNA-modified graphene/platinum nanoparticles hybrid nanosheet with a 1 pM detection limit (Han et al., 2015).

Another multifaceted biosensor target that interacts with p53 to influence senescence, yet with additional roles influencing apoptosis and stem cell functions is telomerase reverse transcriptase (hTERT) (Cong &Shay, 2008). This enzyme acts to extend telomeres, repetitive sequences at the distal ends of chromosomes protecting against replicative genome degradation (Roake & Artandi, 2017). A dramatic consequence of telomerase overexpression is induction of indefinite replication in cultured cells, subverting senescence without necessarily compromising stem cell performance (Shi et al., 2002; Simonsen et al., 2002).

A porphyrin-functionalized graphene nanocomposite for ultrasensitive detection of human telomerase, that presented abundant positively charged domains for DNA capture and amplified the subsequent electrochemiluminescent signal, was described five years ago (Wu et al., 2012). Only recently have a several fluorescent biosensors for telomerase activity emerged. Conveniently dispensing with enzyme-mediated amplification, Hong et al., devised probe-triggered amplification called mimic-hybridization chain reaction consisting of functionalized gold nanoparticles (AuNP) coupled to a GO surface-anchored fluorescent signal. Cellular endocytosis of the biosensor's AuNP/GO/telomerase primer sequence sensitively detected telomerase activity in living cells and appropriately monitored reduced telomerase activity in cells responding to telomerase

inhibitors (Hong et al., 2016). Enhanced nanosensitivity from a GO surface bound hybridization chain reaction strategy, enabled intracellular detection of human Telomerase RNA (hTR) with a 2.7 pM limit (Shi et al., 2016). Within the complex context of urine from bladder cancer patients a GO platform combined with label-free aggregation induced emission flourogen (AIEgen) detected telomerase high selectivity and accuracy (Ou et al., 2017b). A more comprehensive binary assay combined a telomerase extension reaction with miR-21 on a GO platform, whereby nicking enzyme assisted signal amplification and GO adsorption of redundant molecular beacons reduced background noise (Duan et al., 2017). Others have explored nanocarbon structures for telomerase inhibition. Aiming to decrease hTERT activity, plasma activated GO was more effective than plasma activated functionalized multiwall carbon nanotube (f-MWCNT). Such nanocarbon specific inhibition of telomerase activity was attributable to selective binding of activated GO but not f-MWCNT to AtTBR2 protein, a telomere binding protein that forms specific telomeric structures required for telomerase activity (Attri et al., 2017). Deeper understanding of nanomaterial-biomolecular interactions combined with efficient labelling and signal transduction strategies will ensure continued improvements for in vitro/in vivo telomerase assays (Wang et al., 2017a).

3.3 Biosensing cell apoptosis

Apoptosis represents a programmed cell death, often triggered by cytochrome c released from the mitochondrion evoking several other key molecular players (Estaquier et al., 2012). Graphene quantum dot (GQD) adsorption on GO generated a sensitive platform for detecting cytochrome c release in cells (Cao et al., 2017a). Alternatively, an aptameric PEGylated GO nanosensor could visualize cytochrome c in apoptotic HeLa cells (Chen et al., 2015b) to help screen apoptosis-inducing compounds for cancer therapy. Since in certain circumstances GO and rGO induce apoptosis and cell cycle alterations (Kang et al., 2017), graphene-based biosensors can theranostically evaluate apoptotic biomarker levels and induce cancer cell death. Induction of apoptosis in cancer cell lines was confirmed through evaluation of cytochrome c levels (Bahreyni et al., 2017). Exemplifying versatility, one sophisticated targeting strategy involved a GO surface adsorbed mucin 1 (MUC1)-specific aptamer driving cell receptor-mediated endocytosis. Once internalised, a second GO adsorbed vimentin-specific aptamer called NAS-24, drove recognition of vimentin overexpressed by breast cancer cells, triggering apoptosis with cytochrome c release. A third cytochrome c specific fluorolabeled aptamer was subsequently released from the GO sheet with increased fluorescence reflecting cytochrome c accumulation in the cytosol (Bahreyni et al., 2017). Other graphene-based theranostic platforms have been developed for various cancer types, including breast, pancreatic, cervical, lung and liver, and have been tested both *in vitro* and *in vivo* (Chen et al., 2016; Ko et al., 2017; Sun et al., 2017a; Wang et al., 2015b; Xu et al., 2017a; Yin et al., 2017). For cancer-targeting theranostics it is noteworthy that an altered TP53 functional status could render cells more susceptible to the cytotoxicity of oxygen functionalized graphene (Petibone et al., 2017).

Biosensors detecting the cysteine protease Caspase-3, activated during apoptosis can indicate chemotherapeutic efficacy through electrochemical or electrochemiluminescent methods (Khalilzadeh et al., 2017). Ultrasensitive detection of caspase-3 in apoptotic A549 cells (0.5 fM detection limit) was achieved with rGO decorated by gold-nanoparticles, electrochemically deposited on a glassy carbon electrode (Khalilzadeh et al., 2016). The molecular caspase-3 probe used in this biosensing platform was a biotinylated peptide substrate self-assembled on the gold nanoparticles, while composite GO functioned as a signal amplifier due to its

excellent electrical conductivity. GO-assisted signal amplification with a caspase-3 gold electrode biosensor reached a detection limit of 0.06 pg/mL (3.3 fM) (Chen et al., 2015a). Alternatively, optical detection strategies have used covalent attachment of fluorescent peptides containing the caspase-3 enzyme cleavage site in fluorescence quenching GO sheets (Wang et al., 2011). Following enzymatic cleavage, the fluorophore was released from the GO surface, to quantitatively indicate enzyme activity, but the detection limit of 0.4 nM was less than that of electrochemical methods.

Apoptosis inducing factor (AIF), a mitochondrial oxidoreductase inducer of caspase-independent cell death through DNA degradation, has been linked to several malignancies including breast, colon and lung carcinogenesis (Millan & Huerta, 2009). Chemotherapeutic drugs causing apoptosis can induce AIF release from mitochondria (Ostrakhovitch & Cherian, 2005), thus its quantification may monitor treatment progress. Although, commercial graphene-based biosensors for cancer diagnosis have yet to be described, a dual-purpose GO nanosensor for visualization and inhibition of AIF, based on intrinsic GO quenching of fluorescent-labelled DNA probes, identified aberrant apoptotic events in vascular smooth muscle cells (VSMC) of atherosclerotic plaques (Sun et al., 2017b).

Reduced GO platforms can host covalently linked antibodies targeting specific cancer biomarkers; thus a sandwich-type electrochemical biosensor with excellent sensitivity (0.5 fM limit) detected apoptosis relevant proteins BCL2 and BCL2 associated X protein (BAX). Upon antibody binding, the analytes coupled with Ag nanoclusters or Cd quantum dots, for a quantifiable signal via anodic stripping voltammetry (Zhou et al., 2016). Since these homo- or heterodimers of these two proteins tightly regulated apoptosis through opposite mitochondrial membrane functions (Tsujimoto, 1998), their ratio correlated well with cytochrome c release or increase in caspase-3 activity. Administration of increasing doses of the antineoplastic agent nilotinib to K562 CML cells demonstrably increased the BAX/BCL2 ratio and apoptotic cell death.

3.4 Biosensing autophagy

A prominent feature of tumour microenvironments, hypoxia, activates a homeostatic process called autophagy, whereby cytosomal materials are sequestrated and degraded by lysosomes. A key homeo-domain transcription factor, DNA binding Nanog homeobox protein (NANOG) with a role in tumour progression and maintenance of stem cell multilineage differentiation potential, can activate autophagy under hypoxic conditions (Hasmim et al., 2017). Absolute cell levels of the NANOG protein was detected with ultra-sensitivity (0.1-160 pg/mL) with a biosensor using antibody-coated gold nanoparticles deposited on pyrolytic graphite, achieving an order of magnitude higher sensitivity than obtained using more conventional ELISA methods (Chikkaveeraiah et al., 2012). Although graphene may be considered a single layer of graphite, the properties of a graphite electrode versus a graphite electrode coated with graphene were not the same. GO coating of a chemically activated (CA) pencil graphite electrode (PGE) allowed more sensitive voltammetric monitoring of micro RNA miRNA-34a (Isin et al., 2017), a tumour suppressive miRNA that downregulates multiple gene products and can trigger non-canonical autophagy (Gaur et al., 2015). Of note, graphene based materials can themselves induce autophagosome accumulation and lysosome impairment (Ou et al., 2017a), thus the potential for an intracellular biosensor to influence certain measurements mustn't be overlooked.

3.5 Biosensing angiogenesis

Vascular endothelial growth factor (VEGF), a key regulator of angiogenesis, is often evoked by cancer cells to recruit tumour vascularization (Carmeliet, 2005). Some antitumour therapeutic strategies aim to reduce VEGF. Isoform VEGF-A_{165} could be readily adsorbed on bovine serum albumin-capped graphene oxide (BSA-GO), a competitive-binding nanocomposite that trapped VEGF-A_{165} and inhibited proliferation and migration of human umbilical vein endothelial cells (HUVEC) (Lai et al., 2016). Covalently binding a VEGF-specific antibody (bevacizumab) to magnetic GO deposited on a gold electrode (Lin et al., 2015), generated a reusable immunosensor detecting VEGF levels in clinical samples with a broader linear range (31.25–2000 pg mL^{-1}) than classic enzyme linked immunosorbent assays (ELISA), with good correlation detected within a tenth of the time. An aptameric GO-based detection nanoplatform for monitoring prostate cancer, integrating dual evaluation of VEGF and prostate-specific antigen (PSA) demonstrated ELISA-like sensitivity (Pan et al., 2017). It was comprised of a covalently-linked thiol-modified single stranded DNA (ssDNA) probe on a branched polyethyleneimine-modified GO sheet that specifically recognized and sequestered VEGF from the medium. Subsequently, dual-antibody modified poly-L-lactide nanoparticles were added for the capture and immobilization of PSA on the VEGF-containing electrode.

Beyond tumour vascularization, VEGF also participates in vascular pathologies such as ischemia, and VEGF accumulation in poorly-vascularized zones can lead to improved angiogenesis and therapeutic outcomes. VEGF could be readily adsorbed onto the surface of GO, and subsequently used as a theranostic platform in order to promote angiogenesis while at the same time evaluate therapeutic efficacy (Sun et al., 2013).

3.6 Immunosensors and biosensing immunomodulators

Recent success with chimeric antigen receptor (CAR) T-cell antibody mediated cellular therapy highlights the value of measuring target tumour antigens (Calmels et al., 2018). Graphene-based materials are suited for immunosensors given surface modification versatility to immobilize antibodies without losing antigen-recognition ability (Mann et al., 2013). Tumour-associated glycoprotein (TAG-72 or CA72-4) is a gastric cancer-associated biomarker that can be quantified to diagnose and monitor specific immunotherapy. A sandwich-type immunosensor, constructed for the sensitive detection of CA72-4 (0.0003 U/mL), used a glassy carbon electrode coated with tetraethylene pentamine-modified rGO for primary anti-CA72-4 antibody immobilization. Associated PtPd-Fe_3O_4 nanoparticles adsorbed the secondary anti-CA72-4 antibody for subsequent electrochemical quantification (Wu et al., 2015).

The inflammatory cytokine, tumour necrosis alpha (TNF-α), influencing major chronic inflammatory diseases such as atherosclerosis, is a recognized tumour marker. A sandwich-type aptasensor for the sensitive detection of TNF-α (1.64 pg/mL detection limit) used rGO nanosheets functionalized with Ag@Pt nanoparticles to provide an electrochemical readout (Mazloum-Ardakani & Hosseinzadeh, 2016). A more sensitive sandwich-type label-free electrochemical immunosensor (0.1 pg/mL detection limit) was developed with the help of a primary capture anti-TNF-α antibody immobilized on functionalized rGO-modified gold nanoparticles, and a secondary detection anti-TNF-α antibody on a 4-ferrocenylaniline-functionalized rGO for the electrochemical quantification of the ferrocene signal upon target capture (Qi et al., 2016).

Interferon-gamma (IFN-γ) is a soluble cytokine with immunomodulatory and anti-tumour function that can be sensitively quantified with graphene-based biosensors for disease monitoring in a clinical setting. Farid and co-workers developed a sensitive field effect transistor (FET)-based biosensor (1.4 ng/mL detection limit) by immobilizing a modified IFN-γ aptamer on graphene to detect aqueous IFN-γ from charge distribution changes upon analyte binding (Farid et al., 2015). Another, more sensitive sandwich-type electrochemiluminescent sensor, consisted of a primary anti-IFN-γ antibody immobilized on gold nanoparticle-coated magnetic beads attached to a polyaniline nanofiber-GO composite, plus a secondary antibody labelled with CdS quantum dots for generating the signal upon analyte detection. The 30 fg/mL detection limit demonstrated how sophisticated graphene functionalization strategies could improve target sensitivity (Zhu et al., 2016b).

4. Scalable graphene production and material synthesis

For biosensor applications, graphene must ideally be synthesizable on a large scale with highly reproducible control of size, layering, shape and doping, i.e. mixing with foreign atoms, to control properties such as optical excitation wavelength (Bangert et al., 2016). Accelerating production methods beyond the original adhesive tape method (Novoselov et al., 2004) has long been problematical. Although mechanically exfoliated graphene sheets have relatively few defects, low production yields and inadequate control of thickness, size and shape fails to suit biosensors applications (Zhang, 2015).

Instead, novel plasma-based technologies (Levchenko et al., 2016) are among a range of scalable approaches (Tao et al., 2017; Wang et al., 2017b) that offer unique possibilities for enhancing graphene production. Three common forms of graphene product; films, unsupported flakes or supported orientated flakes, each providing particular advantages and disadvantages, are generated by two main approaches: “top-down” and “bottom-up”. The former strategy aims to transform bulky and layered compounds into single and few-layer 2D nanomaterials. Precursors include natural graphite, highly ordered pyrolytic graphite (HOPG) (Seo et al., 2017b) and carbon nanotubes (CNTs) that are physically and chemically exfoliated (Zhang, 2015) or unzipped (Mousavi et al., 2017). A solution-chemistry approach, following oxidation of graphite to graphite oxide with mechanochemical or thermal exfoliation of graphite oxide to GO sheets, is scalable with potentially high yields. GO, a single-layer of graphite oxide with an uncertain pattern of oxygen containing functional groups has excellent electronic, optical, thermal, mechanical and chemical reactivity properties suited for biosensor applications (Chen et al., 2012). Moreover, GO can be reduced, removing the carboxyl, epoxy and hydroxyl oxygen containing functional groups, by chemical, electrochemical, photocatalytic or thermal reduction. Process thoroughness can yield fully reduced graphene oxide (rGO) or partially reduced graphene oxide, with environmentally friendly electrochemical routes being favoured (Zhong & Swager, 2012). Specific organic molecules stabilizing agents can enhance electrochemical liquid phase exfoliation, to adaptably regulate production processes (Haar et al., 2016). Alternatively single-step spark plasma sintering (SPS) can generate highly hydrophobic rGO (Li et al., 2016b) highlighting the impact of the manufacturing process on the qualities of the graphene material obtained.

An advantage of top-down approaches is an ability to control the placement of desired entities. Raman spectroscopy, a powerful, fast non-destructive method to characterise prominent deterministic features, is sensitive to both the phonon and electronic characteristics of graphene-based materials with defects, including

GO and rGO (Wu et al., 2018). Raman analysis of how defects and disorders influence breakage of sp^2 bonds into sp^3 bonds can directly compare different covalent versus non-covalent functionalization techniques. Increased availability of π electrons from restored sp^2 hybridization in non-covalently functionalized rGO featuring a high defect density, conveyed superior charge transfer at the electrode-electrolyte interface (Saha et al., 2017). Such high defect density was found to improve aptamer probe ssDNA interaction via π-π bonds to a rGO surface layered rGO/GO double-layer electrode capable of label-free target cDNA detection (Li et al., 2015). Monitoring sophisticated platform fabrication, combinatorial Raman spectroelectrochemistry obtained real-time measurement of graphene doping molecules, revealing fundamental in-situ information about the molecular species absorbed on the graphene surface (van den Beld et al., 2017).

Bottom-up synthesis approaches aim to directly manufacture ultrathin 2D nanomaterials from different precursors via procedures such as chemical vapour deposition (CVD) for single-layer graphene crystal growth. CVD achieves largely defect-free graphene, continuous up to the centimetre scale, but resorts to high temperature treatments and relatively complicated processes (Berger et al., 2006). Even so, CVD graphene production has been scaled to commercial availability, providing graphene sheets and graphene films transferred onto substrates such as silicon wafers, plastics and glass. Optimizing CVD parameters with respect to H_2 and O_2 ratios, improves nucleation control for tuneable centimetre-sized hexagonal single-crystal graphene layers (Guo et al., 2016). Further reaction condition refinements for faster growth of large graphene single crystals, bearing fewer imperfections e.g. grain boundaries interfering with excellent intrinsic properties, are underway (Zhang et al., 2017). Beyond 2D graphene sheets, popular material forms include graphene nanoribbons (GNRs), narrow strips of graphene with a quasi-one-dimensional nature and graphene quantum dots (GQDs), defined as graphene sheets bearing < 100 nm lateral dimensions, in single-, double- and few- (3 to 10) layer conformations. GNR introduce switching abilities overcoming a zero electronic bandgap limitation of pure native single-layer graphene that renders 2D sheets suboptimal for transistor applications (Hammam et al., 2017; Sprinkle et al., 2010). Fabrication of unidirectional ultra-thin self-aligned GNRs alongside the [0001] direction of SiC substrate, yielded notably superior electrical features in comparison to graphene layers (Jia et al., 2017). GNR alternatively synthesized by multiwall carbon nanotube unzipping with $KMnO_4$ oxidants, formed water-soluble nanoribbons that once centrifuged and dried could make GNR electrodes of very high capacitance (Ping et al., 2017).

Furthering versatility, GQD provide unique and tuneable photoluminescence properties, plus high photo stability, biocompatibility, small size and exceptional physiochemical properties for biosensors (Zheng et al., 2015c). Top-down GQD synthesis involves breaking down large graphene or GO sheets, carbon nanotubes, carbon fibres or graphite into smaller pieces of graphene sheet. Procedural chemical exfoliation (Feng et al., 2014) is being replaced by solvothermal exfoliation (Dang & Kim, 2015), acidic oxidation (Chen et al., 2017a), or electrochemical oxidation (Akkarachanchainon et al., 2017). Abundant raw materials for top-down routes allows large-scale GQD preparation despite complex equipment and critical operating conditions that limit yields and control over the morphology and size distribution of the products. However, in bottom-up approaches precise GQDs can be obtained by step-wise reaction of small molecules e.g. cage-opening of C60 catalysed by ruthenium (Lu et al., 2011), microwave-assisted hydrothermal treatment of carbohydrates (Luo et al., 2016), or carbonizing special organic precursors (Alizadeh & Shokri, 2016). Such GQD routes allow greater control for well-defined molecular size, shape and properties. Bottom-up synthesis methods yield higher quality photoluminescent GQD than top-down approaches (Liu et al., 2011).

5. Chemically-altering graphene to improve biosensor configurations

Biosensor research is currently being enhanced by new nanomaterials with augmented physiochemical properties. Complementing distinct graphene fabrication approaches, new graphene surface chemical derivatization can improve biosensor properties (Liu et al., 2015a). Both covalent and non-covalent graphene functionalization can meet specific biosensor requirements (Georgakilas et al., 2012; Fang & Wang, 2013; Georgakilas et al., 2016). Conveniently, familiar functionalization methods developed for graphite and carbon nanotubes, that endow additional desirable qualities, are often translatable to graphene. Coupling graphene with polymers can provide structures with high sensitivity, selectivity and reproducibility, whilst graphene/metallic nanoparticle composites possess unique physicochemical features that favour sensing applications (Song et al., 2017; Yin et al., 2013). Non-covalent graphene modification with desired functional groups retains integrity of the sp^2-hybridized carbon network and intrinsic chemical, thermal and mechanical properties (Lin & Buehler, 2013).

For graphene-based DNA or RNA sensors, physical adsorption is the simplest immobilization method due to the favourable feature of π–π stacking interaction between the nucleic acid bases of various aptamer probes and the hexagonal graphene lattice. The thermodynamic behaviour at the nucleic acid/graphene surface interface is complex (Ranganathan et al, 2016), nonetheless, experiment broadly corresponds with molecular model predictions (Hughes et al., 2017). Aptamers can have extremely high binding affinity to a variety of target molecules such as proteins, complementary oligonucleotides, cells, or other small molecules. There is similarity to antigen-antibody interactions, but aptamers often possess superior chemical stability to conventional antibodies (Ping et al., 2015), favouring high-performance biosensors (Chen et al., 2017b). Aptasensor platforms comprising non-covalent adsorption of ssDNA and RNA molecules on GO surfaces receive protection from nuclease digestion, improving stability to reduce false positive signals when detecting target molecules (Cui et al., 2013; Tang et al., 2010). Furthermore, taking advantage of nanocomposite versatility, polyanaline (PANI) nanostructures manufactured on a GO substrate improved ssDNA surface coverage and hybridization efficiency to achieve a nanocomposite limit of detection as low as 2.08×10^{-16} M, highlighting nanostructure influence over analyte detection sensitivity (Yang et al., 2014).

Non-covalent functionalisation approaches involving hydrophilic and hydrophobic interactions can also help to functionalize the graphene interface. Amphiphilic molecules (e.g. sodium dodecyl sulphate or hexadecyltrimethylammonium bromide) attached via hydrophobic tails, are good dispersants for graphene in aqueous solution (Ahmad & Thandavan, 2017). Both GO and rGO can be functionalized by hydrophilic polymers (e.g. polyvinyl alcohol, polyethylene glycol) to prevent aggregation in aqueous solution (Liu et al., 2015a).

An undesirable aspect of physical adsorption is that the relatively weak bonds can succumb to stochastic biomolecule detachment from the graphene surface and random molecule orientation may reduce device sensitivity (Zhiani, 2017). Covalent attachment of biomolecules to graphene materials is more stable and especially useful for sensor applications needing long-term modification of the substrate with oriented biomolecules. Furthermore, covalent functionalization may outperform noncovalent functionalization due to improved electron transfer from the aptamer's functional moiety (Lu et al., 2016). Graphene can be covalently functionalized by reaction with unsaturated π-bonds, abundant oxygen-containing groups of GO and heteroatom

doping (Liu et al., 2015a). However, covalent functionalization of graphene may also disrupt sp^2 bonding character and reduce electrical conductivity (Patil et al., 2015) calling for care that graphene functionalization does not compromise electrical performance.

Diazonium chemistry generates highly reactive free radicals for graphene surface addition reactions. The functionalization reaction can be done passively by simple exposing graphene to the diazonium solution or actively by applying the electrochemical reduction. A rapid one-pot synthesis of functionalized graphene was generated by graphite electrochemical exfoliation in the presence of in situ diazonium cations. This was faster than traditional diazonium ion reactions and offered good versatility for further functionalization (Assaud et al., 2016; Kaplan et al., 2017).

GO can be functionalized relatively easily thanks to its abundant oxygen-containing groups. Coupling of biomolecule amine groups with GO functionalities (especially carboxyl) by well-known 1-ethyl-3(3-dimethylaminopropyl)-carbodiimide (EDC) and N-hydroxysulfoccinimide (NHS) protocols, in ambient conditions, can assemble graphene quantum dots (GQDs) via amidic bonds with NH_2 groups in the double-stranded DNA structure (Hu et al., 2016).

Chemical doping with foreign atoms efficiently modifies the intrinsic properties of graphene nanocomposites. Nitrogen and boron atoms are often chosen to fabricate heteroatom-doped graphene due to the similar structure with carbon. Nitrogen doping can significantly enhance electron conductivity, sensitivity and biocompatibility of graphene for biosensing applications (Hao et al., 2017). Note however, that graphene substrate and interface can also strongly influence the doping characteristics (Sforzini et al., 2016).

A direct comparison of covalent grafting versus non-covalent π-π stacking by Dubuisson et al. sought to identify which method produced a clearer signal-to-noise change in bioaffinity events. The dynamic range depended upon the electrode surface qualities and DNA-probe immobilization method. Covalently grafted DNA probes on anodized epitaxial graphene provided a larger dynamic range with a lower detection limit (2×10^{-14} M) and a more sensitive response than the π-π stacked DNA probe (Dubuisson et al., 2011).

The strategy of graphene decoration with inorganic materials (metallic nanoparticles, metal or semi-metal oxides) could provide unique sensing features for biosensor design. The graphene–nanoparticle hybrid structures often exhibit advantages specific to the individual nanoparticles and graphene as well as synergistic properties of the hybrid material (Alfano et al., 2016). For example, graphene sheets decorated with inorganic nanoparticles showed enhanced aqueous dispersion (Li et al., 2015), improved electron transfer between the analyte and the electrode (Pramudita et al., 2017) and better biomolecule immobilization (Su et al., 2017; Yin et al., 2013).

Graphene–metal nanoparticle hybrid structures are often made by reduction of metallic salts using well-known chemical agents such as ethylene glycol, sodium citrate and sodium borohydride. Negatively-charged GO surface functional groups can induce nucleation of positively charged metallic salts, resulting in the successful growth of metal nanoparticles on the GO surface. Accordingly, in situ growth of CuS on the surface of graphene sheets generated nanoparticle-decorated graphene (CuS/GO) composites for a highly sensitive elecrochemical antibody-based bioprobe (Li et al., 2015). Graphene–metal nanoparticle composites can also be produced modifying the nanoparticles with chemical linkers (e.g. mercaptopyridine (Huang et al., 2010) with strong π–π stacking affinity for the graphene surface (Achadu & Nyokong 2017).

Ultrasensitive electrochemical quantification of miRNA from cell lysates could be obtained using bimetallic palladium-platinum (Pd–Pt) supported graphene functionalized screen-printed gold electrodes and

redox-cycling amplification. The Pd/Pt/rGO composite was obtained by a potentiostatic method; applying a potential of -0.2V/SCE to an rGO modified electrode covered by a mixture containing $PtCl_6^-$ and $PdCl_6^-$ (Cheng et al., 2014). Increasingly, graphene-nanoparticle composite structures can be synthesized via electrochemical techniques that advantageously control the density and size of the nanoparticles (Tandel et al., 2017).

Graphene functionalization remains crucial for manufacturing highly specific trustworthy biosensors. Reproducibility of chemically and non-chemically altered graphene species is a key aspect to be aforethought early in design. Different types of functionalization can lead to dramatic differences in maintenance of the graphene lattice structure (Fig. 2) (Peng et al., 2015). Functionalization procedures need to follow standard protocols strictly to minimise the variations reported between runs (Pykal et al., 2016)

6. Advantages of 2D nanomaterials for biointerfaces

The increased electrode surface area of 2D nanomaterials provides more reactive sites for post-detection signal amperometric transduction. Greater total current response for an analyte in solution is particularly beneficial for sensing analytes at low concentrations. Noteworthy, is the significant importance of establishing clean electrodes before graphene modification (Fig. 3). Modifying glassy carbon electrode (GCE) with chitosan functionalized rGO, produced an electrochemical biosensing platform transducing signals via differential pulse voltammetry that could directly analyse total analyte concentrations in cell lysates. The sensitivity and detection range exceeded ELISA methods, showing promise for complex real samples (Wei et al., 2014).

Resorting to rGO could enhance electrochemical signals compared to GO (Fig. 4), however GO retains advantages for certain contexts (Loo et al., 2012) and increased discrimination among different ssDNA targets (Giovanni et al., 2012). Fundamentally, the GO/GCE electrochemical response when ssDNA interacts with GO included a decrease in the voltammetric peak currents of a negatively charged redox probe (e.g $[Fe(CN)_6]^{3-/4-}$), proportional to the amount of ssDNA (Fig. 5A). Proposedly, this reflects repellence of $[Fe(CN)_6]^{3-/4-}$ by the negatively charged phosphate backbone of the ssDNA (Benvidi et al., 2015). When measuring the behaviour of GO/GCE in the presence of the same redox probe by electrochemical impedance spectroscopy (EIS), the charge transfer resistance increases, as seen by a larger Nyquist plot semicycle diameter (Figs. 5B, 5D). Hybridization of the complementary target DNA sequence evokes higher repulsion between the negative charge of the dsDNA and the redox probe anions. For studies using a covalently attached DNA probe, this causes a further decrease of the peak current of the redox probe (Fig. 5C) and an increase of the charge transfer resistance (Fig. 5D). This behaviour is more pronounced when increasing the target DNA concentration (Figs. 5E, 5F) making this electrochemical approach suitable for quantitative DNA sensing. N.B. non-covalently adsorbed nucleotide aptamer probes may evoke a decreased charge transfer resistance due to partial release of the hybridized DNA from the electrode surface (Bonanni et al., 2011; Giovanni et al., 2012; Campos et al., 2018).

Using electrochemical techniques for detection of low abundant diffusing molecules is problematic because for each encounter with the electrode only one or a very few of the redox-active molecule electrons contributes to the measured current. Protein redox centres are often buried within folded polypeptide shells, resulting in a poor electron charge transfer rate at the protein surface. Thus when wanting to measure individual molecules, an electron-transfer detector needs to obtain a charge amplification, increasing the number of electrons involved, fortunately, GO and rGO were both suitable for this purpose (Gupta & Irihamye, 2015).

Graphene can form strong hydrophobic interactions, providing protein adsorption, whilst concurrently providing high electron mobility to help tunnel electron transfer between the redox centre of the protein and the electrode surface (Settu et al., 2017). For example, graphene sheets functionalized on both sides by non-covalently attached single protein molecules of microperoxidase-11 (MP-11), formed a graphene-sandwiched nanoparticle of high charge and low density that promptly migrated in an electric field with an increased electrode collision frequency. The collision frequency was a function of protein concentration; it was possible to estimate the number of MP-11 molecules on a single nanosheet was in the range of 10^5 ±18. In this manner, protein molecules attached to the surface of graphene nanosheets could provide an ultrasensitive electrochemical detection platform (Li et al., 2014). Notably, MP-11 molecules enhanced aqueous solubility, reduced graphene-sheet aggregation and could covalently bind a range of analyte-capturing molecules, including DNA, enzymes and antibodies, providing scope for implementing this interface in a versatile range of rapid and highly sensitive sensors (Wang et al., 2015a).

7. The quest for high analyte sensitivity

Excellent nucleotide detection has been achieved with electrochemical sensors, especially those using rGO electrodes, however signal amplification could further enhance the sensitivity and dynamic range. Small size deterministic molecules may exist at a relatively low abundance e.g. miRNAs are very influential in cancer and key indicators of stem cell differentiation, capable of influencing bone regeneration (Chang et al., 2017). A number of alternative "beyond graphene" 2D materials have been considered for use as biosensors (Shavanova et al., 2016) detecting a broad range of analytes including miRNA. Conveniently, miRNA analyte similarity allows a reasonably direct performance comparison for biosensors adopting different materials, in particular different GO composites (Table 2). A material showing excellent performance is molybdenum disulphide MoS_2 (Gan et al., 2017) that like graphene can respond with ultrasensitive and selective optical and/or electronical signal changes to nucleotide analytes. Pristine 2D MoS_2 is nonetheless also susceptible to aggregation and restacking, so it is often combined with other nanoscale conductors.

A specific feature of miRNA is that it is derived from regions of RNA transcripts that fold back on themselves to form short hairpin loops. These in turn can be subjected to an enzyme-free amplification method termed Catalysed Hairpin Assembly (CHA) that adapts rules governing nucleic acid hybridisation to signal amplification (Li et al., 2011). Through further elaboration, enzyme-assisted nucleic acid amplification provided a highly sensitive electrochemical sensor for miRNA detection based composites of tungsten oxide and reduced graphene oxide (WO_3-rGO) coupled to CHA target recycling and enzyme signal amplification (Shuai et al., 2016). By combining high selectivity from CHA target miRNA recycling, with enzymatic electrochemical-chemical redox cycling reactions at the electrode, a remarkably low detection limit of 0.05 fM was achieved. Such high selectivity and sensitivity would render the protocol suitable for quantifying miRNA in complex real-life samples. Probing subtle changes in interface impedance upon bioaffinity recognition events at the surface/electrolyte interface can suffice for the technique of Electrochemical Impedance Spectroscopy (EIS) (Li et al., 2016a), especially if biomolecule immobilization occupies a large surface area and the signal transducing material has high conductivity (Bonanni & Pumera, 2011), making graphene an ideal surface for impedimetric biosensing. Of note, EIS is a non-invasive technique, bypassing the need to modify the biomolecule with labels (Dubuisson et al., 2011). When measuring charge transfer resistance (Rct) with redox-active species in the

electrolyte, there can be controversy as to exactly how bioaffinity events alter Rct. GO adsorbs loose linear single-stranded nucleic acid structures (e.g. ssDNA), but efficient shielding within the densely negatively charged phosphate backbone of dsDNA means GO has relatively low interaction with more rigidly structured double-stranded DNA (dsDNA). Graphene-associated unbound ssDNA analyte ligand interacting with the target probe can form double-stranded DNA (dsDNA) that more readily detaches from the surface than non-interacting graphene-associated unbound ssDNA analyte ligand. Thus ssDNA hybridization to dsDNA would decrease the Rct value (Yang et al., 2013b). Nonetheless, with certain modified graphene substrates, dsDNA could remain on the biosensor surface, causing an increased impedimetric value. Hybridization between complementary sequences may induce a rise of negative surface charge, which may repel a negatively charged redox probe (e.g. ferricyanide ions) and cause an increase in Rct. This working principle was recently illustrated by Seo et al. developing an electrochemical genosensor using a substrate of ambient-air synthesized graphene films from a renewable soybean oil precursor. The EIS response to complementary miRNAs indicated a dynamic range of 0.1pM to 1nM, with a detection limit of 8.64 x 10^{-14} M (Seo et al., 2017a).

Combining graphene with the conductive polymer polyaniline (PANI) generated a DNA probe platform of enhanced interaction with the glassy carbon electrodes. Altering the platform substrate composition in terms of PANI/graphene mass ratios influenced the decisive forces for dsDNA retention or release from the surface (Zheng et al., 2015b). Substrate modulation ultimately resulted in a highly efficient DNA sensor with a wide detection range of 0.01 pM to 1 μM that could discriminate single nucleotide polymorphisms (SNPs).

Graphene's high carrier density, typically ~2x10^{11} cm^{-2} for suspended single layers and an extremely high electron mobility of ~200,000 cm^2 V^{-1} s^{-1} even at room temperature without doping, leads to high electron mobility and transconductance far higher than any conventional semiconductor (Du et al., 2008), promising a high signal-to-noise detection ratio. Ambipolar field-effect characteristics mean that adsorption of either electron withdrawing or donating groups can lead to "chemical gating" of the material, readily monitored by resistive-type sensors (Chen et al., 2010). Graphene's high surface atom density renders its electron transport network exquisitely sensitive to adsorbed molecule interactions, structural differences arising from the starting material and also diverse production processes that may alter the inherent electrochemistry (Ambrosi et al., 2014).

FET sensors that detect changes in the conductance of ion surface doped graphene from charged analytes in aqueous solutions provide advantages over enzymatic electrochemical sensors, since they do not involve irreversible consumption of the analyte and suffer less from electroactive species interference. Aptameric graphene bound DNA that avidly binds low-charged small-molecule analytes can extend the advantages of FET sensors to analytes including organic molecules and peptides that don't necessarily directly induce changes in surface charge. Thus, small molecule steroid hormones could be measured at clinically relevant concentrations with an estimated detection limit < 50 nM (Wang et al., 2015a). Therefore, the choice of bio-recognition layer in biologically sensitive field-effect transistors (BioFETs) is critical to overall biosensor performance (Pachauri & Ingebrandt, 2016). Sensitivity is also influenced by more accurate graphene fabrication, and a novel directional transfer technique based on CVD grown single-layer graphene could extend DNA detection sensitivity to concentrations as low as 10 fM, with single-base pair discernment between complementary and non-complementary DNA sequences (Zheng et al., 2015a). DNA displacement strand probes and FET sensors provide highly efficient and specific single-nucleotide polymorphism (SNP) detection (Hwang et al., 2016).

Enhanced DNA hybridizations can be achieved using peptide nucleic acids (PNA) as capture molecules. The PNA nucleotide has a negatively charged phosphate backbone replaced by a neutral peptide backbone that diminishes repulsion between the two hybridized strands causing stronger aptamer-analyte interactions to reduce background signals. This also reflects the PNA probe's high sequence specific affinity and stoichiometric stability derived from rigid amino bonds, flexible aminoethyl linkers and intra-molecular hydrogen bonding. Replacing a prior complex top-down fabrication with a bottom-up approach, Cai et al conveniently made rGO-based FET biosensors with ultrasensitive label-free detection of DNA achieving a 100 fM detection limit, ten-fold more sensitive than earlier DNA-DNA hybridization FET biosensors (Cai et al., 2014).

Control of precise graphene geometry could influence electrode configuration to further enhance sensitivity (Kasputis et al., 2015). Vertically oriented deposition of graphene sheets labelled with gold nanoparticle-antibody conjugates enhanced the surface area accessible to the analyte, leading to a low selective protein detection limit of 13 pM (Yang et al., 2013a). Thus high analyte sensitivity could be achieved through various electrochemical approaches that targeted a wide range of analytes, providing the adaptability necessary for graphene-based biosensors to meet the multiparametric demands of ATMP potency assays.

8. From electrochemical to GO quenched optical biosensors

Multiparameter analysis for cancer diagnosis and stem cell potency assays makes diverse colours particularly desirable for improved specificity and efficient detection. Moreover, nanotechnology can achieve new levels of optical performance, meeting more stringent demands for robust and precise measurement of spatial and temporal parameters. Chief among enabling technologies is Förster (fluorescence) resonance energy transfer (FRET), an electromagnetic energy transfer phenomenon between two fluorescently labelled molecules obeying energy conservation laws. Transfer of photonic energy between an excited donor and acceptor is facilitated when they share analogous resonance frequencies, whereby the donor dipole radiates photons at the same frequency by which they can be adsorbed by the acceptor. Notably, FRET does not represent independent donor light emission and acceptor adsorption, rather, a coupled distance-dependent interactions between the two dipoles. An effectively coupled resonance transition between the fluorophore pair quenches the donor (emission) radiance via an irreversible and radiationless FRET mechanism, with transferred energy dissipated as heat (Obeng et al., 2016). The 1 to 10 nm FRET radius between the interacting dipoles befits biomolecular interactions and nanosecond resonance energy transfer allows time-resolved analysis of biomolecular conformation and localization. Accompanying advances in fluorescent protein characterisation and sophisticated imaging techniques have allowed powerful exploitation of the FRET phenomenon.

GO properties are highly suited to the FRET phenomenon. Pure graphene completely composed of sp^2-hybridized carbon atoms exhibits no fluorescence due to a zero optical bandgap. However, exfoliated GO or rGO bear heterogeneous atomic and electronic structures that impart intrinsic and tuneable fluorescence (Loh et al., 2010). Matching the FRET prerequisite of spectral overlap, the emission of 6-carboxyfluorescein (6-FAM) is compatible with the absorbance of GO. Thus GO could replace a second fluorescent dye to serve as the FRET acceptor dipole. Moreover, GO may serve as a broad spectrum quencher for a range of dyes, facilitating development of a multiplex sensing FRET system. A GO-aptamer based FRET biosensor achieved rapid and specific determination of vascular endothelial growth factor (VEGF) in complex samples, including serum with

detection limits of 2.56 x 10^{-10} M (Wang & Si, 2013). In the ground state nanoprobe biosensor, π-π stacking interactions between GO and an oligonucleotide aptamer tagged with 6-FAM fluorophore lie within the close dipole distance needed for efficient quenching. In the presence of VEGF analyte, the selective complex formed with the single strand DNA aptamer generated a more rigid G-quadruplex DNA structure that relinquished the non-covalent π-π interactions with the GO surface, thus releasing tagged 6-FAM from GO quenching, restoring fluorophore fluorescence in a manner quantitatively proportional to the amount of VEGF. Following the above principles with elegant exploitation of hybridizations between unfolded single-stranded collagen fibrils and complementary collagen triple helix sequences, a GO-FRET based biosensor was able to specifically detect unfolded collagen fragments, as found in some pathological processes, at nM levels (Sun et al., 2016b).

More recently, nanomaterials for a FRET based biosensor repertoire have included transition metal dichalcogenides (TMDs) e.g. MnO_2, MoS_2, $MoSe_2$ and WS_2 recognised for good biocompatibility, large surface areas and unique optical properties (Tian et al., 2017). In comparison to pristine graphene, GO may have weaker quenching ability due to changes in carbon hybridization from sp^2 to sp^3, nonetheless, these suffice for a rapid 100% quenching response over a quenching distance as far as 23 nm. In contrast to GO, rGO has a better quenching ability from a higher sp^2 carbon ratio. Parameters including dopants, functionalized groups and lateral size can determine the electronic transitions governing fluorescent peak outcomes, for example incubating GO in aqueous HNO_3 to enrich it with carboxyl groups, altered the photoluminescence fingerprint with subsequent stronger emission intensities at the long excitation-wavelength range (Li et al., 2012).

Since the GO bandgap reflects the mixture of sp^2 and sp^3 carbon atoms, the electronic band structure can be tailored by modifying the sp^2/sp^3 carbon atom ratio, thus allowing the fluorescence to be tuned towards the near-infrared wavelength. Graphene quantum dots, like GO, have a modifiable fluorescence emission, e.g. nitrogen-doped GQDs show an emission with better photostability. Changes in GQD size modulate the electronic structure and shift fluorescence wavelengths. Responsiveness to longer wavelengths, including near-infrared excitation, reduces cellular phototoxicity for selective biological imaging. GO is well-complemented by two-photon luminescence platforms that can influence GO photoluminescence emission spectra by varying the excitation wavelength, without changing the GQD chemical composition or size. The small size of GQD, allowing membrane permeability and excitation-wavelength-dependent emission favours their use for in vitro and in vivo bioimaging. A broad range of optical sensor design strategies are accommodated by the ability of GO to act as a fluorescent label, as a donor in charge transfer, as a donor or acceptor in FRET, and as photostable GQD (Zheng &Wu, 2017).

Improved methods of GQD synthesis, removing impurities that reduce charge transfer with interacting target molecules and novel nanocomposites are promoting prospects for more stringent and effective biosensor designs (Liu et al., 2018). Overcoming the overtly extreme conductivity of pristine graphene, many alternative graphene-like 2D materials introduce a small bandgap, or energy barrier for electron flow, that provides an "off" state for greater control of electron flow. In particular, 2D molybdenum disulphide (MoS_2) is drawing attention as a stable inorganic graphene analogue that can complement graphene for optoelectronics since its bandgap qualities lead to strong photoluminescence emission (Gan et al., 2017). A photodetector based on graphene/MoS_2 heterostructures could achieve higher photoresponsivity than 10^7 A/W whilst retaining its unique ultrathin nature (Zhang et al., 2014b) and graphene/MoS_2 structures could provide ultrasensitive detection of DNA hybridization (Loan et al., 2014).

9. Future Perspectives for real-time and point of care devices

The roadmap for graphene related materials is broad, with rapid development inviting expectation of low-cost, ultra-sensitive, ultra-compact, label-free, on chip, high-throughput and real-time sensing platforms (Ferrari et al., 2015). Limiting overview of how graphene based biosensors may enhance human cell therapy to proof of principle studies targeting key biomolecules and a description of key chemical properties for versatile biosensor design, risks overlooking the truly transformative value that such biosensors may bring by enabling real-time and point of care measurement. The World Health Organisation ASSURED guidelines (affordable, sensitive, specific, user-friendly, rapid and robust, equipment-free and delivered) for point of care devices, define expectations that in some cases are already largely met by some of the examples above.

Assisting technologies include lab-on-a-chip (LOC) integrated diagnostic devices incorporating microfluidic control for low sample volumes to provide miniaturization, portability and faster analysis time. Notably, GO based membrane can itself improve microfluidic flow control in such integrated platforms (Gaughran et al., 2016) with tunable GO membrane thickness controllable via vacuum filtration synthesis methods. With landmark examples of transgenic stem cell therapy treating genetic disease affecting skin sub-epidermis (Hirsch et al., 2017), it is relevant that with intrinsic flexibility, graphene could be incorporated in wearable polymeric chips, such as the skin biosensor developed by Pu et al., for continuous non-invasive glucose monitoring of subcutaneous interstitial fluid. Notably, the single layer graphene device provided an improved selective detection limit of 1.44 mg/dL, in contrast to a 90 mg/dL limit for a configuration without graphene (Pu et al., 2016). Similarly, understanding the therapeutic effectiveness of ß-cell replacement therapy in the treatment of diabetes (Rickels et al., 2018) is likely to benefit from wearable electrochemical devices that can measure glucose in human perspiration (Lee et al., 2016) with the increased simplicity and autonomy such POC biosensors can bring (da Silva et al., 2017; Syedmoradi et al., 2017). The excellent conductive properties of graphene can allow passive low power detection approaches. Modulation of the electrical conductivity of a graphene film upon bacteria binding antimicrobial peptide biorecognition elements resulted in continuous and remote monitoring of breath and saliva in a tooth enamel interfaced biosensor with detection down to a single bacterium (Mannoor et al., 2012).

All the above successful examples may beg the question, why are commercial graphene based biosensors rare and not in routine use? The answer partly lies in the raised concern for product quality and testing performance of more widely available POC biosensors. Implementation within in a human cell therapy context is complex because of the need for integration within the design, operation and management of clinical workflows to ensure timely accessible assays; with results possibly used in real time, to guide treatment. This may paradoxically introduce additional procedural demands that require improved medical-record systems to capture results and make them available as critical parameters. Despite graphene being a material of extreme properties, hyperbole needs to be tamed by appreciation of the many engineering hurdles preventing prompt adoption of graphene-based biosensor in clinical cell therapy settings. Integration of biosensors into miniaturized systems requires further research development, especially for greater consistency and reliability. Manufacture remains problematical since functionalized graphene can be sensitive to humidity and temperature. Use of internal recalibration controls may help mitigate such problems, but it may also be advisable to adopt careful handling methods akin to operation management approaches of the fresh food industry (Diakosavvas et al., 2017). The extent to which label-free measurements truly don't stress or modify the biological sample will

require comprehensive analysis to exclude assay limitations. Implantable theranostic devices will require long-term toxicity studies that extend to metabolic pathways and environmental impact. Biosensor design sustainability issues will become increasingly important for progress from an advanced preclinical laboratory stage to biosensor validation using large patient cohorts (Morales-Narváez et al., 2017).

Fortunately, progress in nanomaterial surface characterisation that improves understanding of parameters dictating biosensor performance is evolving with improved cellular characterisation determining how cell based therapy might enhance medical intervention. Combined, these advances are synergistic for implementation of new clinical approaches needed to address our most challenging diseases. A commercially available graphene field effect transistor (G-FET) biosensing chip, the Agile R100 based on functionalized graphene has been reported to robustly measure clinically relevant target molecules (peptides, proteins, antibodies) in real time for dynamic pM level characterisation in complex media (Lerner et al., 2016). Indeed, G-FETs are likely to play a significant role in next generation affinity sensors, given demonstrable high sensitivity for a broad range of target molecule sizes, multiplex assay potential and reduced manufacturing costs compared to optical nanolithographic approaches (Xu et al., 2017b). Since screen printing electrode (SPE) technology is one of the most widely applied techniques for large-scale production of low-cost disposable electrochemical biosensors, incorporation of graphene in various fabrication printing inks represents another keenly pursued approach. SPE can achieve successful detection of picogram levels of target molecules (Teixeira et al., 2014), yet some drawbacks from unpredictable results arising from auxiliary ink ingredients (polymeric binders, stabilizers, etc.) warrant further methodological research and development (Syedmoradi et al., 2017).

Focused development of biosensor design needs to be fostered through interactions between scientists and clinicians and industrial providers. Despite considerable challenges, the rapid progress underlying the current status of graphene-based biosensor technology and human cell therapy presents cooperative advantages and optimism for synergistic benefit and success.

10. Summary and Conclusions

Since the prized achievement of one atom thick single-layer graphene in 2004 (Geim & Novoselov, 2007), widespread interest in exploitation of its qualities has included detection of biological substances (Yu et al., 2017). In-depth understanding of the interplay between biosystems and nanomaterials and the corresponding action mechanism are providing valuable examples for nanobiotechnology, yet also introducing requirement for improved nomenclature (Sanchez et al., 2012) and classifications (Wick et al., 2014). Cancer research and regenerative medicine have need of flexible and robust methods to enhance measurement speed, accuracy, precision, specificity, sensitivity and dynamic range for a wide range of valuable biomarkers (Hematti, 2016). Biosensors based on 2D nanomaterials represent a major advance for reducing complex analysis to common device platforms rather than diverse instruments. Perhaps the most vexing concern regarding graphene based biosensors remains reliability and stability, with known issues including biorecognition elements of poor chemical stability, short lifetime and high cost. Careful and convenient manipulation procedures to prevent degradative loss of bioactivity are required. In this regard advances in aptamer chemistry are providing new bioreceptors for POC biosensors (Hori et al., 2018; da Silva et al., 2017) and the potential for GO to protect absorbed nucleic acids from enzymatic degradation make it a favourable platform for the increased use of both

mRNA and non-coding RNA to characterise therapeutic stem cell status (Murgia et al., 2016; Fatima et al., 2017: Chang et al., 2018).

Examples of graphene-based biosensors that characterise expression of molecules relevant to cancer diagnostics and human cell therapy assays demonstrate degrees of sensitivity that are consistent with or superior to conventional methods of measurement. Advances in nanomaterial surface characterisation and nanocomposite design are enhancing graphene based biosensors in a manner that will improve the quality control of manufacturing methods and improve subsequent reproducibility and reliability. By way of recent example, use of copper-dielectric biosensor chips instead of gold for plasmonic biosensors demonstrated excellent performance for quantitative detection of oligonucleotides captured by a GO probe linking layer, providing chips that could be manufactured with industry standard complementary metal oxide semiconductor (CMOS) processes (Stebunov et al., 2018). The prospects of label-free sensing and the possibility of continuous and prompt real-time measurement proffer additional benefits, highlighting an exciting opportunity for graphene based sensors to advance human cell therapy.

Acknowledgements

We thank Diana Becheru for help with the preparation of this manuscript. This work was supported by a grant of the National Authority for Scientific Research and Innovation, Operational Program Competitiveness Axis 1 - Section E, Program co- financed from European Regional Development Fund "Investments for your future" under the project number 154 / 25.11.2016, P_37_221 / 2015.

Disclosure of potential conflicts of interest

The authors declare no potential conflict of interest.

References

Achadu O., Nyokong T., 2017. Dyes Pigm. 145, 189-201.

Afsahi S., Lerner M.B., Goldstein J.M., Lee J., Tang X., Bagarozzi D.A., Pan D., Locascio L., Walker A., Barron F., Goldsmith B.R., 2018. Biosens. Bioelectron. 100, 85-88.

Ahmad H., Thandavan T.M.K., 2017. Opt. Mater. 73, 441-448.

Akhavan O., 2016. J. Mater. Chem. B. 4, 3169-3190.

Akkarachanchainon N., Rattanawaleedirojn P., Chailapakul O., Rodthongkum N., 2017. Talanta. 165, 692-701.

Alfano B., Polichetti T., Mauriello M., Miglietta M.L., Ricciardella F., Massera E., Di Francia G., 2016. Sens. Actuators B Chem. 222, 1032-1042.

Ali M.A., Singh C., Mondal K., Srivastava S., Sharma A., Malhotra B.D., 2016. ACS Appl. Mater. Interfaces. 8, 7646-7656.

Alizadeh T., Shokri M., 2016. Sens. Actuators B Chem. 222, 728-734.

Amărandi R.-M., Becheru D. F., Vlăsceanu G. M., Ioniță M. and Burns J. S., 2018 Biomed Resesarch International, in press.

Ambrosi A., Chua C., Bonanni A., Pumera M., 2014. Chem. Rev. 114, 7150-7188.

Assaud L., Massonnet N., Evrard D., Vergnes H., Salvagnac L., Conédéra V., Noé L., Monthioux M., Gros P., Temple-Boyer P., Caussat B., 2016. J. Electroanal. Chem. 771, 73-79.

Attri P., Gaur J., Choi S., Kim M., Bhatia R., Kumar N., Park J. H., Cho A. E., Choi E. H. and Lee W., 2017. Sci Rep 7, 2636.

Azimzadeh M., Rahaie M., Nasirizadeh N., Ashtari K., Naderi-Manesh H., 2016. Biosens. Bioelectron. 77, 99-106.

Bahreyni A., Yazdian-Robati R., Hashemitabar S., Ramezani M., Ramezani P., Abnous K., Taghdisi S., 2017. Int. J. Pharm. 526, 391-399.

Bangert U., Pierce W., Boothroyd C., Pan C., Gwilliam R., 2016. Sci. Rep. 6, 27090.

Benvidi A., Rajabzadeh N., Molaye Zahedi H., Mazloum-Ardakani M., Heidari M.M., Hosseinzadeh L., 2015. Talanta. 137, 80-86.

Berger C., Song Z., Li X., Wu X., Brown N., Naud C., Mayou D., Li T., Hass J., Marchenkov A., Conrad E., First P., de Heer W., 2006. Science. 312, 1191-1196.

Bhatnagar D., Kumar V., Kumar A., Kaur I., 2016. Biosens. Bioelectron. 79, 495-499.

Bianying F., Linjie G., Lihua W., Fan L., Jianxin L., Jimin G., Chunhai F., Qing H., 2013. Anal. Chem. 85, 7732-7737.

Bollella P., Fusco G., Tortolini C., Sanzò G., Favero G., Gorton L., Antiochia R., 2017. Biosens. Bioelectron. 89, 152-166.

Bonanni A., Pumera M., 2011. ACS Nano. 5, 2356-2361.

Bressan E., Ferroni L., Gardin C., Sbricoli L., Gobbato L., Ludovichetti F.S., Tocco I., Carraro A., Piattelli A., Zavan B., 2014. J. Transl. Med. 12, 469.

Buscaglia L.E., Li Y., 2011. Chinese journal of cancer. 30, 371-380.

Cai B., Wang S., Huang L., Ning Y., Zhang Z., Zhang G., 2014. ACS Nano. 8, 2632-2638.

Cai B., Huang L., Zhang H., Sun Z., Zhang Z. and Zhang G.-J., 2015. Biosensors and Bioelectronics 74, 329-334.

Cai B., Guo S. and Li Y., 2018. Analytical Methods

Calmels B., Mfarrej B. and Chabannon C., 2018. Drug Discov Today

Cao L., Li X., Qin L., Kang S.-Z., Li G., 2017a. J. Mat. Chem. B. 5, 6300-6306.

Cao Y., Dong H., Yang Z., Zhong X., Chen Y., Dai W., Zhang X., 2017b. ACS Appl. Mater. Interfaces. 9, 159-166.

Carmeliet P., 2005. Oncology. 69 Suppl 3, 4-10.

Catalanotto C., Cogoni C. and Zardo G., 2016. IJMS 17, 1712.

Chan J., Krichevsky A., Kosik K., 2005. Cancer Res. 65, 6029-6033.

Chan K. F., Lim H. N., Shams N., Jayabal S., Pandikumar A. and Huang N. M., 2016. Mater Sci Eng C Mater Biol Appl 58, 666-674.

Chang C. C., Venø M. T., Chen L., Ditzel N., Le D. Q. S., Dillschneider P., Kassem M. and Kjems J., 2017. Mol Ther 26, 593-605.

Chauhan N., Maekawa T., Kumar D.N.S., 2017. J. Mater. Res. 32, 2860-2882.

Chen C.-H., Hu S., Shih J.-F., Yang C.-Y., Luo Y.-W., Jhang R.-H., Chiang C.-M., Hung Y., Jr., 2017a. Sci. Rep. 7, 3908.

Chen D., Tang L., Li J., 2010. Chem. Soc. Rev. 39, 3157-3180.

Chen D., Feng H., Li J., 2012. Chem. Rev. 112, 6027-6053.

Chen F., Liu Y., Liao R., Gong H., Chen C., Chen X., Cai C., 2017b. Anal. Chim. Acta. 985, 141-147.

Chen H., Zhang J., Gao Y., Liu S., Koh K., Zhu X., Yin Y., 2015a. Biosens. Bioelectron. 68, 777-782.

Chen T., Tian X., Liu C., Ge J., Chu X., Li Y., 2015b. J. Am. Chem. Soc. 137, 982-989.

Chen Y.W., Liu T.Y., Chen P.J., Chang P.H., Chen S.Y., 2016. Small. 12, 1458-1468.

Cheng F., Zhang J., He T., Shi J., Abdel-Halim E., Zhu J., 2014. Analyst. 139, 3860-3865.

Chikkaveeraiah B. V., Soldà A., Choudhary D., Maran F. and Rusling J. F., 2012. Nanomedicine (Lond) 7, 957-965.

Cohen J. D., Li L., Wang Y., Thoburn C., Afsari B., Danilova L., Douville C., Javed A. A., Wong F., Mattox A., Hruban R. H., Wolfgang C. L., Goggins M. G., Dal Molin M., Wang T. L., Roden R., Klein A. P., Ptak J., Dobbyn L., Schaefer J., Silliman N., Popoli M., Vogelstein J. T., Browne J. D., Schoen R. E., Brand R. E., Tie J., Gibbs P., Wong H. L., Mansfield A. S., Jen J., Hanash S. M., Falconi M., Allen P. J., Zhou S., Bettegowda C., Diaz L., Tomasetti C., Kinzler K. W., Vogelstein B., Lennon A. M. and Papadopoulos N., 2018. Science (epub ahead of print).

Cong Y. and Shay J. W., 2008. Cell Res 18, 725-732.

Cruz S., Girão A., Gonçalves G., Marques P., 2016. Sensors. 16, 137.

Cui L., Chen Z., Zhu Z., Lin X., Chen X., Yang C., 2013. Anal. Chem. 85, 2269-2275.

Cui L., Lin X., Lin N., Song Y., Zhu Z., Chen X., Yang C., 2012. Chem. Commun. 48, 194-196.

da Silva E. T. S. G., Souto D. E. P., Barragan J. T. C., de F Giarola J., de Moraes A. and Kubota L. T., 2017. ChemElectroChem 4, 778-794.

Dang D., Kim E., 2015. Nanoscale Res. Lett. 10.

Devadas B., Rajkumar M., Electrochem … S. M. C.-I. J. and 2012, 2012. electrochemsci.org

Diakosavvas et al., OECD 2017. OECD Green Growth Studies, OECD Publishing, Paris. http://dx.doi.org/10.1787/9789264278530-en

Dong H., Zhang J., Ju H., Lu H., Wang S., Jin S., Hao K., Du H., Zhang X., 2012. Anal. Chem. 84, 4587-4593.

Dong X., Shi Y., Huang W., Chen P., Li L., 2010. Adv. Mater. 22, 1649-1653.

Drusco A., Croce C., 2017. Adv. Cancer Res. 135, 1-24.

Du D., Wang L., Shao Y., Wang J., Engelhard M., Lin Y., 2011. Anal. Chem. 83, 746-752.

Du X., Skachko I., Barker A. and Andrei E. Y., 2008. Nat Nanotechnol 3, 491-495.

Duan R., Zhang Z., Zheng F., Wang L., Guo J., Zhang T., Dai X., Zhang S., Yang D., Kuang R., Wang G., He C., Hakeem A., Shu C., Yin P., Lou X., Zeng F., Liang H. and Xia F., 2017. ACS Appl Mater Interfaces 9, 23420-23427.

Dubuisson E., Yang Z., Loh K., 2011. Anal. Chem. 83, 2452-2460.

Estaquier J., Vallette F., Vayssiere J., Mignotte B., 2012. Adv. Exp. Med. Biol. 942, 157-183.

Esteban-Fernández de Ávila B., Araque E., Campuzano S., Pedrero M., Dalkiran B., Barderas R., Villalonga R., Kiliç E., Pingarrón J., 2015. Anal. Chem. 87, 2290-2298.

Fang Y., Wang E., 2013. Chem. Commun. 49, 9526-9539.

Farid S., Meshik X., Choi M., Mukherjee S., Lan Y., Parikh D., Poduri S., Baterdene U., Huang C.-E., Wang Y.Y., Burke P., Dutta M., Stroscio M.A., 2015. Biosens. Bioelectron. 71, 294-299.

Fatima F., Ekstrom K., Nazarenko I., Maugeri M., Valadi H., Hill A. F., Camussi G. and Nawaz M., 2017. Front Genet 8, 161.

Feng H., Wu Y., Li J., 2014. Small. 10, 2233-2238.

Ferrari A., Bonaccorso F., Fal'ko V., Novoselov K., Roche S., Bøggild P., Borini S., Koppens F., Palermo V., Pugno N., Garrido J., Sordan R., Bianco A., Ballerini L., Prato M., Lidorikis E., Kivioja J., Marinelli C., Ryhänen T., Morpurgo A., Coleman J., Nicolosi V., Colombo L., Fert A., Garcia-Hernandez M., Bachtold A., Schneider G., Guinea F., Dekker C., Barbone M., Sun Z., Galiotis C., Grigorenko A., Konstantatos G., Kis A., Katsnelson M., Vandersypen L., Loiseau A., Morandi V., Neumaier D., Treossi E., Pellegrini V., Polini M., Tredicucci A., Williams G., Hong B., Ahn J., Kim J., Zirath H., van Wees B., van der Zant H., Occhipinti L., Di Matteo A., Kinloch I., Seyller T., Quesnel E., Feng X., Teo K., Rupesinghe N., Hakonen P., Neil S., Tannock Q., Löfwander T., Kinaret J., 2015. Nanoscale. 7, 4598-4810.

Fischbach M., Bluestone J., Lim W., 2013. Sci. Transl. Med. 5, 179ps7.

Foroutan T., Nazemi N., Tavana M., Kassaee M., Motamedi E., Soieshargh S., Zare Zardini H., 2017. J. Biomed. Mater. Res. A.

Furukawa K., Ueno Y., Takamura M., Hibino H., 2016. ACS Sens. 1, 710-716.

Gan X., Zhao H., Quan X., 2017. Biosens. Bioelectron. 89, 56-71.

Gaughran J., Boyle D., Murphy J., Kelly R. and Ducrée J., 2016. Microsystems & Nanoengineering 2, 16008.

Gaur S., Wen Y., Song J. H., Parikh N. U., Mangala L. S., Blessing A. M., Ivan C., Wu S. Y., Varkaris A., Shi Y., Lopez-Berestein G., Frigo D. E., Sood A. K. and Gallick G. E., 2015. Oncotarget 6, 29161-29177.

Geim A., Novoselov K., 2007. Nat. Mater. 6, 183-191.

Georgakilas V., Otyepka M., Bourlinos A. B., Chandra V., Kim N., Kemp K. C., Hobza P., Zboril R. and Kim K. S., 2012. Chem Rev 112, 6156-6214.

Georgakilas V., Tiwari J. N., Kemp K. C., Perman J. A., Bourlinos A. B., Kim K. S. and Zboril R., 2016. Chem Rev 116, 5464-5519.

Giovanni M., Bonanni A. and Pumera M., 2012. Analyst 137, 580-583.

Gómez-Barrena E., Rosset P., Lozano D., Stanovici J., Ermthaller C., Gerbhard F., 2015. Bone. 70, 93-101.

Guo W., Jing F., Xiao J., Zhou C., Lin Y., Wang S., 2016. Adv. Mater. 28, 3152-3158.

Gupta S., Irihamye A., 2015. AIP Adv. 5, 037106.

Ha N. R., Jung I. P., La I. J., Jung H. S. and Yoon M. Y., 2017. Sci Rep 7, 40305.

Hirsch T., Rothoeft T., Teig N., Bauer J. W., Pellegrini G., De Rosa L., Scaglione D., Reichelt J., Klausegger A., Kneisz D., Romano O., Secone Seconetti A., Contin R., Enzo E., Jurman I., Carulli S., Jacobsen F., Luecke T., Lehnhardt M., Fischer M., Kueckelhaus M., Quaglino D., Morgante M., Bicciato S., Bondanza S. and De Luca M., 2017. Nature 551, 327-332.

Hammam A.M.M., Schmidt M.E., Muruganathan M., Mizuta H., 2017. Carbon. 121, 399-407.

Han Y., Chabu J., Hu S., Deng L., Liu Y., Guo S., 2015. Chemistry. 21, 13045-13051.

Hao N., Zhang X., Zhou Z., Qian J., Liu Q., Chen S., Zhang Y., Wang K., 2017. Sens. Actuators B Chem. 250, 476-483.

Hasmim M., Janji B., Khaled M., Noman M. Z., Louache F., Bordereaux D., Abderamane A., Baud V., Mami-Chouaib F. and Chouaib S., 2017. J Immunol 198, 1423-1428.

He L., Pagneux Q., Larroulet I., Serrano A. Y., Pesquera A., Zurutuza A., Mandler D., Boukherroub R. and Szunerits S., 2017. Biosens Bioelectron 89, 606-611.

Hematti P., 2016. Transfusion. 56, 32S-35S.

Hermenean A., Codreanu A., Herman H., Balta C., Rosu M., Mihali C. V., Ivan A., Dinescu S., Ionita M. and Costache M., 2017. Sci Rep 7, 16641.

Hong C., Baek A., Hah S., Jung W., Kim D., 2016a. Anal. Chem. 88, 2999-3003.

Hong M., Xu L., Xue Q., Li L. and Tang B., 2016b. Anal Chem 88, 12177-12182.

Hori S. I., Herrera A., Rossi J. J. and Zhou J., 2018. Cancers (Basel) 10,

Hu T., Zhang L., Wen W., Zhang X., Wang S., 2016. Biosens. Bioelectron. 77, 451-456.

Huang J., Zhang L., Chen B., Ji N., Chen F., Zhang Y., Zhang Z., 2010. Nanoscale. 2, 2733-2738.

Hughes Z. E., Wei G., Drew K. L. M., Colombi Ciacchi L. and Walsh T. R., 2017. Langmuir 33, 10193-10204.

Hwang D., Kim H., Li F., Park J., Kim D., Park J., Han H., Byun J., Lee Y., Jeong J., Char K., Lee D., 2017. Biomaterials. 121, 144-154.

Hwang M., Landon P., Lee J., Choi D., Mo A., Glinsky G., Lal R., 2016. Proc. Natl. Acad. Sci. U.S.A. 113, 7088-7093.

Haar S., Bruna M., Lian J., Tomarchio F., Olivier Y., Mazzaro R., Morandi V., Moran J., Ferrari A., Beljonne D., Ciesielski A., Samorì P., 2016. J. Phys. Chem. Lett. 7, 2714-2721.

Ioniţă M., Vlăsceanu G., Watzlawek A., Voicu S., JS B., H I., 2017. Compos. B Eng. 121, 34-57.

Isin D., Eksin E. and Erdem A., 2017. Mater Sci Eng C Mater Biol Appl 75, 1242-1249.

Janegitz B., Silva T., Wong A., Ribovski L., Vicentini F., Taboada Sotomayor M., Fatibello-Filho O., 2017. Biosens. Bioelectron. 89, 224-233.

Jayanthi V.S.P.K.Sankara A., Das A.B., Saxena U., 2017. Biosens. Bioelectron. 91, 15-23.

Jia Y., Guo L., Lin J., Yang J., Chen X., 2017. Carbon. 114, 585-590.

Jung Y., Lee T., Shin E., Kim B., 2013. Sci. Rep. 3, 3367.

Justino C.I.L., Gomes A.R., Freitas A.C., Duarte A.C., Rocha-Santos T.A.P., 2017. Trends Anal. Chem. 91, 53-66.

Kang Y., Liu J., Wu J., Yin Q., Liang H., Chen A., Shao L., 2017. Int. J. Nanomedicine. 12, 5501-5510.

Kaplan A., Yuan Z., Benck J.D., Govind Rajan A., Chu X.S., Wang Q.H., Strano M.S., 2017. Chem. Soc. Rev. 46, 4530-4571.

Kasputis T., Pieper A., Rodenhausen K., Schmidt D., Sekora D., Rice C., Schubert E., Schubert M., Pannier A., 2015. Acta Biomater. 18, 88-99.

Khalilzadeh B., Shadjou N., Charoudeh H.N., Rashidi M.-R., 2017. Microchim. Acta. 184, 3651-3662.

Khalilzadeh B., Shadjou N., Afsharan H., Eskandani M., Nozad Charoudeh H., Rashidi M., 2016. Bioimpacts. 6, 135-147.

Kilic T., Kaplan M., Demiroglu S., Erdem A., Ozsoz M., 2016. J. Electrochem. Soc. 163, B227-B233.

Kinoshita T., Yip K. W., Spence T. and Liu F. F., 2017. J Hum Genet 62, 67-74.

Kim T.-H., Lee T., El-Said W., Choi J.-W., 2015. Materials. 8, 8674-8690.

Ko N.R., Nafiujjaman M., Lee J.S., Lim H.N., Lee Y.K., Kwon I.K., 2017. RSC Adv. 7, 11420-11427.

Lai P., Chen C., Wei S., Lin T., Jian H., Lai I., Mao J., Hsu P., Lin H., Tzou W., Chen S., Harroun S., Lai J., Huang C., 2016. Biomaterials. 109, 12-22.

Lee H., Choi T. K., Lee Y. B., Cho H. R., Ghaffari R., Wang L., Choi H. J., Chung T. D., Lu N., Hyeon T., Choi S. H. and Kim D. H., 2016. Nat Nanotechnol 11, 566-572.

Lerner M. B., Pan D., Gao Y., Locascio L. E., Lee K.-Y., Nokes J., Afsahi S., Lerner J. D., Walker A. and Collins P. G., 2017. Sensors and Actuators B: Chemical 239, 1261-1267.

Levchenko I., Ostrikov K.K., Zheng J., Li X., Keidar M., K B.K.T., 2016. Nanoscale. 8, 10511-10527.

Li B., Ellington A., Chen X., 2011. Nucleic Acids Res. 39, e110.

Li B., Pan G., Avent N. D., Lowry R. B., Madgett T. E. and Waines P. L., 2015. Biosens Bioelectron 72, 313-319.

Li M., Cushing S. K., Zhou X., Guo S. and Wu N., 2012. J. Mater. Chem. 22, 23374.

Li D., Liu J., Barrow C., Yang W., 2014. Chem. Commun. 50, 8197-8200.

Li L., Zhang L., Yu J., Ge S., Song X., 2015. Biosens. Bioelectron. 71, 108-114.

Li Y., Wang Q., Zhang Y., Deng D., He H., Luo L., Wang Z., 2016a. Colloids Surf. B. Biointerfaces. 145, 160-166.

Li Z., Tang X., Zhu W., Thompson B., Huang M., Yang J., Hu X., Khor K., 2016b. ACS Appl. Mater. Interfaces. 8, 10985-10994.

Lian Y., He F., Wang H., Tong F., 2015. Biosens. Bioelectron. 65, 314-319.

Lin C., Wei K., Liao S., Huang C., Sun C., Wu P., Lu Y., Yang H., Ma C., 2015. Biosens. Bioelectron. 67, 431-437.

Lin S., Buehler M., 2013. Nanotechnology. 24, 165702.

Ling K., Jiang H., Li Y., Tao X., Qiu C., Li F., 2016. Biosens. Bioelectron. 86, 8-13.

Liu D., Chen X., Hu Y., Sun T., Song Z., Zheng Y., Cao Y., Cai Z., Cao M., Peng L., Huang Y., Du L., Yang W., Chen G., Wei D., Wee A. T. S. and Wei D., 2018. Nat Commun 9, 193.

Liu H., Zhang L., Yan M., Yu J., 2017. J. Mater. Chem. B. 5, 6437-6450.

Liu H., Li L., Wang Q., Duan L., Tang B., 2014. Anal. Chem. 86, 5487-5493.

Liu J., Liu Z., Barrow C., Yang W., 2015a. Anal. Chim. Acta. 859, 1-19.

Liu L., Song C., Zhang Z., Yang J., Zhou L., Zhang X. and Xie G., 2015b. Biosensors and Bioelectronics 70, 351-357.

Liu R., Wu D., Feng X., Müllen K., 2011. J. Am. Chem. Soc. 133, 15221-15223.

Liu Y., Dong X., Chen P., 2012. Chem. Soc. Rev. 41, 2283-2307.

Loan P., Zhang W., Lin C., Wei K., Li L., Chen C., 2014. Adv. Mater. 26, 4838-4844.

Loh K., Bao Q., Eda G., Chhowalla M., 2010. Nat. Chem. 2, 1015-1024.

Loo A. H., Bonanni A. and Pumera M., 2012. Nanoscale 4, 143-147.

Lu C., Jimmy Huang P.J., Ying Y., Liu J., 2016. Biosens. Bioelectron. 79, 244-250.

Lu C., Yang H., Zhu C., Chen X., Chen G., 2009. Angew. Chem. Int. Ed. 48, 4785-4787.

Lu J., Yeo P., Gan C., Wu P., Loh K., 2011. Nat. Nanotechnol. 6, 247-252.

Lu J., Wu L., Hu Y., Wang S., Guo Z., 2017. J. Electrochem. Soc. 164, B421-B426.

Luo Z., Qi G., Chen K., Zou M., Yuwen L., 2016, 2016. Adv. Funct. Mater. 26, 2739-2744.

Ma H., Wu D., Cui Z., Li Y., Zhang Y., Du B. and Wei Q., 2013. Analytical Letters

Ma W., Sun M., Fu P., Li S., Xu L., Kuang H., Xu C., 2017. Adv. Mater.

Maity N., Mandal A., Polymer A. K. N. and 2016, 2016. Elsevier

Majd S. M., Salimi A. and Ghasemi F., 2018. Biosensors and Bioelectronics

Malekpour H., Ramnani P., Srinivasan S., Balasubramanian G., Nika D. L., Mulchandani A., Lake R. K. and Balandin A. A., 2016. Nanoscale 8, 14608-14616.

Mann J.A., Alava T., Craighead H.G., Dichtel W.R., 2013. Angew. Chem. Int. Ed. 52, 3177-3180.

Mannoor M. S., Tao H., Clayton J. D., Sengupta A., Kaplan D. L., Naik R. R., Verma N., Omenetto F. G. and McAlpine M. C., 2012. Nat Commun 3, 763.

Mao S., Yu K., Chang J., Steeber D., Ocola L., Chen J., 2013. Sci. Rep. 3, 1696.

Mazloum-Ardakani M., Hosseinzadeh L., 2016. J. Electrochem. Soc. 163, B119-B124.

McKee C., Chaudhry G., 2017. Colloids Surf. B. Biointerfaces. 159, 62-77.

Meng F., Henson R., Wehbe-Janek H., Ghoshal K., Jacob S., Patel T., 2007. Gastroenterology. 133, 647-658.

Menaa F., Abdelghani A., Menaa B., 2015. J. Tissue Eng. Regen. Med. 9, 1321-1338.

Miao X., Ning X., Li Z. and Cheng Z., 2016. Scientific reports 6, 32358.

Millan A., Huerta S., 2009. J. Surg. Res. 151, 163-170.

Mohanty N., Berry V., 2008. Nano Lett. 8, 4469-4476.

Montes-Navajas P., Asenjo N. G., Santamaría R., Menéndez R., Corma A. and García H., 2013. Langmuir 29, 13443-13448.

Morales-Narváez E., Baptista-Pires L., Zamora-Gálvez A. and Merkoçi A., 2017. Adv Mater 29, 1604905

Mousavi H., Jalilvand S., Kurdestany J.M., Grabowski M., 2017. Physica E Low Dimens. Sys. Nanostruct. 94, 87-91.

Muazim K., Hussain Z., 2017. Mater. Sci. Eng. C Mater. Biol. Appl. 76, 1274-1288.

Mulvaney S., Stine R., Long N., Tamanaha C., Sheehan P., 2014. BioTechniques. 57, 21-30.

Murgia A., Veronesi E., Candini O., Caselli A., D'souza N., Rasini V., Giorgini A., Catani F., Iughetti L., Dominici M., Burns J., 2016. PLoS One. 11, e0163629.

Maartens J., De-Juan-Pardo E., Wunner F., Simula A., Voelcker N., Barry S., Hutmacher D., 2017. Expert Opin. Biol. Ther. 17, 1221-1233.

Novoselov K.S., Geim A.K., Morozov S.V., Jiang D., Zhang Y., Dubonos S.V., Grigorieva I.V., Firsov A.A., 2004. Science. 306, 666-669.

Obeng E.M., Dullah E.C., Danquah M.K., Budiman C., Ongkudon C.M., 2016. Anal. Methods. 8, 5323-5337.

Ossonon B., Bélanger D., 2017. Carbon. 111, 83-93.

Ostrakhovitch E., Cherian M., 2005. J. Cell. Biochem. 95, 1120-1134.

Ou L., Lin S., Song B., Liu J., Lai R. and Shao L., 2017a. Int J Nanomedicine 12, 6633-6646.

Ou X., Hong F., Zhang Z., Cheng Y., Zhao Z., Gao P., Lou X., Xia F. and Wang S., 2017b. Biosens Bioelectron 89, 417-421.

Pachauri V., Ingebrandt S., 2016. Essays Biochem. 60, 81-90.

Pan L., Kuo S., Lin T., Lin C., Fang P., Yang H., 2017. Biosens. Bioelectron. 89, 598-605.

Patil A.V., Fernandes F.B., Bueno P.R., Davis J.J., 2015. Bioanalysis. 7, 725-742.

Pei S., Wei Q., Huang K., Cheng H. M. and Ren W., 2018. Nat Commun 9, 145.

Peng S., Liu C. and Fan X., 2015. Integrated Ferroelectronics 163, 42-53.

Petibone D. M., Mustafa T., Bourdo S. E., Lafont A., Ding W., Karmakar A., Nima Z. A., Watanabe F., Casciano D., Morris S. M., Dobrovolsky V. N. and Biris A. S., 2017. J Appl Toxicol 37, 1333-1345.

Ping J., Zhou Y., Wu Y., Papper V., Boujday S., Marks R.S., Steele T.W.J., 2015. Biosens. Bioelectron. 64, 373-385.

Ping Y., Zhang Y., Gong Y., Cao B., Fu Q., Acta C.P.-E., 2017. Electrochim. Acta. 250, 84-90.

Pramudita J.C., Pontiroli D., Magnani G., Gaboardi M., Milanese C., Bertoni G., Sharma N., Riccò M., 2017. Electrochim. Acta. 250, 212-218.

Pryzhkova M.V., 2013. Stem Cells Transl. Med. 2, 376-383.

Pu Z., Zou C., Wang R., Lai X., Yu H., Xu K. and Li D., 2016. Biomicrofluidics 10, 011910.

Pykal M., Jurečka P., Karlický F., Otyepka M., 2016. Phys. Chem. Chem. Phys. 18, 6351-6372.

Qi M., Zhang Y., Cao C., Zhang M., Liu S., Liu G., 2016. Anal. Chem. 88, 9614-9621.

Qin Y., Zhou Z.W., Pan S.T., He Z.X., Zhang X., Qiu J.X., Duan W., Yang T., Zhou S.F., 2015. Toxicology. 327, 62-76.

Ranganathan S. V., Halvorsen K., Myers C. A., Robertson N. M., Yigit M. V. and Chen A. A., 2016. Langmuir 32, 6028-6034.

Reinhardt H. C. and Schumacher B., 2012. Trends Genet 28, 128-136.

Rafiq Q., Twomey K., Kulik M., Leschke C., O'Dea J., Callens S., Gentili C., Barry F., Murphy M., 2016. Regen. Med. 11, 351-354.

Ricci R., Leite N., da-Silva N., Pacheco-Soares C., Canevari R., Marciano F., Webster T., Lobo A., 2017. Mater. Sci. Eng. C Mater. Biol. Appl. 78, 341-348.

Rickels M. R., Stock P. G., de Koning E. J. P., Piemonti L., Pratschke J., Alejandro R., Bellin M. D., Berney T., Choudhary P., Johnson P. R., Kandaswamy R., Kay T. W. H., Keymeulen B., Kudva Y. C., Latres E., Langer R. M., Lehmann R., Ludwig B., Markmann J. F., Marinac M., Odorico J. S., Pattou F., Senior P. A., Shaw J. A. M., Vantyghem M. C. and White S., 2018. Transplantation

Roake C. M. and Artandi S. E., 2017. Cold Spring Harb Perspect Med 7, 1-16.

Ryoo S., Lee J., Yeo J., Na H., Kim Y., Jang H., Lee J., Han S., Lee Y., Kim V., Min D., 2013. ACS Nano. 7, 5882-5891.

Saha S., Samanta P., Chandra Murmu N. and Kuila T., 2017. Phys Chem Chem Phys 19, 28588-28595.

Sanchez V. C., Jachak A., Hurt R. H. and Kane A. B., 2012. Chem Res Toxicol 25, 15-34.

Senbanjo L., Chellaiah M., 2017. Front. Cell Dev. Biol. 5, 18.

Seo D., Pineda S., Fang J., Gozukara Y., Yick S., Bendavid A., Lam S., Murdock A., Murphy A., Han Z., Ostrikov K., 2017a. Nat. Commun. 8, 14217.

Seo W., White D., Star A., 2017b. Chemistry. 23, 5652-5657.

Settu K., Liu J., Chen C., Tsai J., 2017. Anal. Biochem. 534, 99-107.

Sforzini J., Hapala P., Franke M., van Straaten G., Stöhr A., Link S., Soubatch S., Jelínek P., Lee T., Starke U., Švec M., Bocquet F., Tautz F., 2016. Phys. Rev. Lett. 116, 126805.

Shang N.G., Papakonstantinou P., McMullan M., Chu M., Stamboulis A., Potenza A., Dhesi S.S., Marchetto H., 2008. Adv. Funct. Mater. 18, 3506-3514.

Shavanova K., Bakakina Y., Burkova I., Shtepliuk I., Viter R., Ubelis A., Beni V., Starodub N., Yakimova R. and Khranovskyy V., 2016. Sensors (Basel) 16, 223.

Shi S., Gronthos S., Chen S., Reddi A., Counter C. M., Robey P. G. and Wang C. Y., 2002. Nat Biotechnol 20, 587-591.

Shi Z., Zhang X., Cheng R., Li B. and Jin Y., 2016. Analyst 141, 2727-2732.

Shin Y., Kang S., Lee J., Kim B., Hong S., Han D., 2017. J. Biomater. Sci. Polym. Ed., 1-13.

Shuai H.-L., Huang K.-J., Xing L.-L., Chen Y.-X., 2016. Biosens. Bioelectron. 86, 337-345.

Simonsen J. L., Rosada C., Serakinci N., Justesen J., Stenderup K., Rattan S. I., Jensen T. G. and Kassem M., 2002. Nat Biotechnol 20, 592-596.

Song H., Li X., Cui P., Guo S., Liu W., Wang X., 2017. Sens. Actuators B Chem. 244, 124-130.

Spike B. T. and Wahl G. M., 2011. Genes & Cancer 2, 404-419.

Sprinkle M., Ruan M., Hu Y., Hankinson J., Rubio-Roy M., Zhang B., Wu X., Berger C., de Heer W.A., 2010. Nat. Nanotechnol. 5, 727-731.

Stebunov Y. V., Aftenieva O. A., Arsenin A. V. and Volkov V. S., 2015. ACS Appl Mater Interfaces 7, 21727-21734.

Stebunov Y. V., Yakubovsky D. I., Fedyanin D. Y., Arsenin A. V. and Volkov V. S., 2018. Langmuir 34, 4681-4687.

Su D., Zhang Y., Wang Z., Wan Q., Yang N., 2017. Carbon. 117, 313-321.

Sun B.M., Wu J.R., Cui S.B., Zhu H.H., An W., Fu Q.G., Shao C.W., Yao A.H., Chen B.D., Shi D.L., 2017a. Nano Res. 10, 37-48.

Sun C., Wakefield D. L., Han Y., Muller D. A., Holowka D. A., Baird B. A. and Dichtel W. R., 2016a. Chem 1, 273-286.

Sun L., Zhang Y., Wang Y., Yang Y., Zhang C., Weng X., Zhu S. and Yuan X., 2018. Nanoscale

Sun X., Fan J., Zhang Y., Chen H., Zhao Y., Xiao J., 2016b. Biosens. Bioelectron. 79, 15-21.

Sun Y., Gao W., Zhao Y., Cao W., Liu Z., Cui G., Tong L., Lei F., Tang B., 2017b. Anal. Chem. 89, 4642-4647.

Sun Z., Huang P., Tong G., Lin J., Jin A., Rong P., Zhu L., Nie L., Niu G., Cao F., Chen X., 2013. Nanoscale. 5, 6857-6866.

Suvarnaphaet P., Pechprasarn S., 2017. Sensors. 17, 2161.

Syedmoradi L., Daneshpour M., Alvandipour M., Gomez F., Hajghassem H., Omidfar K., 2017. Biosens. Bioelectron. 87, 373-387.

Tandel R., Teradal N., Satpati A., Jaldappagari S., 2017. Chin. Chem. Lett. 28, 1429-1437.

Tang Z., Wu H., Cort J., Buchko G., Zhang Y., Shao Y., Aksay I., Liu J., Lin Y., 2010. Small. 6, 1205-1209.

Tao H., Zhang Y., Gao Y., Sun Z., Yan C., Texter J., 2017. Phys. Chem. Chem. Phys. 19, 921-960.

Teixeira S., Conlan R. S., Guy O. J. and Sales M. G. F., 2014. Journal of Materials Chemistry B 2, 1852-1865.

Tian F., Lyu J., Shi J., Yang M., 2017. Biosens. Bioelectron. 89, 123-135.

Tsujimoto Y., 1998. Genes Cells. 3, 697-707.

Uder B., Gao H., Kunnas P., Jonge N. D. and Hartmann U., 2018. Nanoscale

van den Beld W. T., Odijk M., Vervuurt R. H., Weber J. W., Bol A. A., van den Berg A. and Eijkel J. C., 2017. Sci Rep 7, 45080.

Wang C., Kim J., Zhu Y., Yang J., Lee G.-H., Lee S., Yu J., Pei R., Liu G., Nuckolls C., Hone J., Lin Q., 2015a. Biosens. Bioelectron. 71, 222-229.

Wang H., Zhang Q., Chu X., Chen T., Ge J., Yu R., 2011. Angew. Chem. Int. Ed. 50, 7065-7069.

Wang H., Wang Y., Liu S., Yu J., Xu W., Guo Y., Huang J., 2014. RSC Adv. 4, 60987-60994.

Wang L., Ma F., Tang B. and Zhang C., 2017a. Chemical Science 8, 2495-2502.

Wang L., Xiong Q., Xiao F., Duan H., 2017b. Biosens. Bioelectron. 89, 136-151.

Wang S., Si S., 2013. Appl. Spectrosc. 67, 1270-1274.

Wang X.J., Sun X., He H., Yang H., Lao J., Song Y.Z., Xia Y.Q., Xu H., Zhang X.D., Huang F., 2015b. J. Mater. Chem. B. 3, 3583-3590.

Wang X.-Y., Narita A. and Müllen K., 2017c. Nat. Rev. Chem. 2, 0100.

Webber M., Appel E., Meijer E., Langer R., 2016. Nat. Mater. 15, 13-26.

Wei C., Liu Z., Jiang F., Zeng B., Huang M. and Yu D., 2017. Cell Prolif 50,

Wei H., Sun J. J., Xie Y., Lin C. G., Wang Y. M., Yin W. H. and Chen G. N., 2007. Anal Chim Acta 588, 297-303.

Wei T., Tu W., Zhao B., Lan Y., Bao J., Dai Z., 2014. Sci. Rep. 4, 3982.

Wick P., Louw-Gaume A. E., Kucki M., Krug H. F., Kostarelos K., Fadeel B., Dawson K. A., Salvati A., Vázquez E., Ballerini L., Tretiach M., Benfenati F., Flahaut E., Gauthier L., Prato M. and Bianco A., 2014. Angew Chem Int Ed Engl 53, 7714-7718.

Wu X., Chai Y., Yuan R., Zhuo Y. and Chen Y., 2014. Sensors and Actuators B: Chemical 203, 296-302.

Wu D., Guo Z., Liu Y., Guo A., Lou W., Fan D., Wei Q., 2015. Talanta. 134, 305-309.

Wu J. B., Lin M. L., Cong X., Liu H. N. and Tan P. H., 2018. Chem Soc Rev

Wu L., Wang J., Feng L., Ren J., Wei W. and Qu X., 2012. Adv Mater 24, 2447-2452.

Xu Z.Q., Wu S.C., Huang G.C., Ding H.W., Gui R.J., Zhu B.H., 2017a. Mater. Lett. 195, 131-135.

Xu S., Zhan J., Man B., Jiang S., Yue W., Gao S., Guo C., Liu H., Li Z., Wang J. and Zhou Y., 2017b. Nat Commun 8, 14902.

Yang G., Li L., Rana R.K., Zhu J.-J., 2013a. Carbon. 61, 357-366.

Yang T., Li Q., Li X., Wang X., Du M., Jiao K., 2013b. Biosens. Bioelectron. 42, 415-418.

Yang T., Meng L., Zhao J., Wang X. and Jiao K., 2014. ACS Appl Mater Interfaces 6, 19050-19056.

Yew Y.T., Loo A.H., Sofer Z., Klímová K., Pumera M., 2017. Appl. Mater. Today. 7, 138-143.

Yin F., Hu K., Chen Y., Yu M., Wang D., Wang Q., Yong K., Lu F., Liang Y., Li Z., 2017. Theranostics. 7, 1133-1148.

Yin H., Zhou Y., Zhang H., Meng X., Ai S., 2012. Biosens. Bioelectron. 33, 247-253.

Yin P., Kim T., Choi J., Lee K., 2013. Phys. Chem. Chem. Phys. 15, 12785-12799.

Yu X., Zhang W., Zhang P., Su Z., 2017. Biosens. Bioelectron. 89, 72-84.

Zhang H., 2015. ACS Nano. 9, 9451-9469.

Zhang L.-N., Deng H.-H., Lin F.-L., Xu X.-W., Weng S.-H., Liu A.-L., Lin X.-H., Xia X.-H., Chen W., 2014a. Anal. Chem. 86, 2711-2718.

Zhang W., Chuu C., Huang J., Chen C., Tsai M., Chang Y., Liang C., Chen Y., Chueh Y., He J., Chou M., Li L., 2014b. Sci. Rep. 4, 3826.

Zhang Z., Luo L., Chen G., Ding Y., Deng D., Fan C., 2014c. Biosens. Bioelectron. 60, 161-166.

Zhang Z., Xu X., Qiu L., Wang S., Wu T., Ding F., Peng H., Liu K., 2017. Adv. Sci. 4, 1700087.

Zhao Q., Zhou Y., Li Y., Gu W., Zhang Q., Liu J., 2016. Anal. Chem. 88, 1892-1899.

Zheng C., Huang L., Zhang H., Sun Z., Zhang Z., Zhang G., 2015a. ACS Appl. Mater. Interfaces. 7, 16953-16959.

Zheng P. and Wu N., 2017. Chem Asian J 12, 2343-2353.

Zheng Q., Wu H., Shen Z., Gao W., Yu Y., Ma Y., Guang W., Guo Q., Yan R., Wang J., Ding K., 2015b. Analyst. 140, 6660-6670.

Zheng X., Ananthanarayanan A., Luo K., Chen P., 2015c. Small. 11, 1620-1636.

Zhiani R., 2017. Appl. Surf. Sci. 409, 35-44.

Zhong Y., Swager T., 2012. J. Am. Chem. Soc. 134, 17896-17899.

Zhou H., Wang X., Yu P., Chen X. and Mao L., 2012. Analyst 137, 305-308.

Zhou L., Mao H., Wu C., Tang L., Wu Z., Sun H., Zhang H., Zhou H., Jia C., Jin Q., Chen X., Zhao J., 2017. Biosens. Bioelectron. 87, 701-707.

Zhou S., Wang Y., Zhu J., 2016. ACS Appl. Mater. Interfaces. 8, 7674-7682.

Zhu W., Su X., Gao X., Dai Z. and Zou X., 2014. Biosensors and Bioelectronics 53, 414-419.

Zhu D., Wang L., Xu X., Jiang W., 2016a. Biosens. Bioelectron. 75, 155-160.

Zhu M., Tang Y., Wen Q., Li J., Yang P., 2016b. Microchim. Acta. 183, 1739-1748.

Zhu D., Liu W., Zhao D., Hao Q., Li J., Huang J., Shi J., Chao J., Su S. and Wang L., 2017. ACS applied materials & interfaces 9, 35597-35603.

Table and Figure Legends

Table 1

Graphene-based biosensors performance for detection of several biomarkers

Abbreviations:

AAB (anti-apolipoprotein B 100); Ab (antibody); afGQDs (amine functionalized graphene quantum dots); anti-cTnI (anti-cardiac Troponin I antibody); BSA (bovine serum albumin); cTnI (cardiac marker antigen Troponin I); DPV (differential pulse voltammetry); EIS (electrochemical impedance spectroscopy); FET (field effect transistor); FRET (fluorescence resonance energy transfer); GA (glutaraldehyde);
GCE (glassy carbon electrode); GO (graphene oxide); GQDs (graphene quantum dots); Gr (graphene produced by chemical vapour deposition); H1, H2 (hairpin DNA); HBV (hepatitis B virus); HRP (horseradish peroxidase**);** HSA (human serum albumin), STA (Streptavidin); IgG (immunoglobulin G); IgM (immunoglobulin M); LbL (layer-by-layer); LDL (low density lipoprotein); MCH (diethylpyrocarbonate 6-mercaptohexanol); PGE (pencil graphite electrode); phospho-p53^{392} (phosphorylated p53 protein at Ser392); PNA (peptide nucleic acid); PSA (prostate specific antigen);RCA (rolling circle amplification); RGO (reduced graphene oxide); SPCE (screen printed carbon electrode); SWV (square wave voltammetry); TRA (tryptamine); VEGFR2 (vascular endothelial growth factor receptor 2); VG (vertically-oriented graphene).

Table 2

Performances of different nanomaterials-based biosensors for miRNA biomarkers detection.

Abbreviations:

AuNPs (gold nanoparticles); *cDNA* (target DNA); *CHA* (catalyzed hairpin assembly reaction);
CV (cyclic voltammetry); DPV (differential pulse voltammetry);
ECL (Electrochemiluminescence); **Fe_3O_4@Au MNPs**- *cDNA* (magnetite@gold magnetic nanoparticles-capture DNA);
FET (field effect transistor); **GNRs** (gold nanorods);
GO (graphene oxide); **GQDs** (graphene quantum dots); *HCPs* (hairpin-shaped capture probes);
HCR (hybridization chain reaction); *MB* (methylene blue); **MoS_2** (molybdenum disulphide)**ND**s (nanodiamonds); *NF* (nafion); *OB* (Oracet Blue); **PdNPs** (palladium nanoparticles); *PNA* (peptide nucleic acid); **rGO** (reduced graphene oxide); *SH-CPs* (Thiolated helper capture probe); *SH-DNA* (Thiolated helper DNA probe); *ssDNA***PbS**+*ssDNA***CdS** (**QD**s) (affinity probes labeled with single stranded DNA lead sulphide and cadmium sulphide quantum dots) **SWCNTs-ox** (oxidized single-walled carbon nanotubes); SWV (square wave voltammetry); *Thi* (thionine); *TSPs* (tetrahedron-structured probes); (*sDNA*&l*uminol*)@**GO** (signal unit GO labeled by luminol and signal DNA).

Fig. 1

Phenotypes and molecular mediators influencing stem cells and cancer cells in their respective microenvironments. Molecules detectable by carbon or graphene based biosensors related to key functional processes of; (1) Proliferation, (2) Senescence, (3) Apoptosis, (4) Autophagy, (5) Angiogenesis, (6) Immunity; include AIF (apoptosis inducing factor), Bax (BCL-2 associated X protein), Bcl-2 (B-cell lymphoma 2),CA72-4 (cancer antigen 72-4), Caspase-3, Cytochrome C, IFN-γ (interferon gamma), miR-21 (microRNA 21), NANOG,

p53, hTERT (telomerase reverse transcriptase), TNF-α (tumour necrosis factor alpha), VEGF-A (vascular endothelial growth factor A).

Fig. 2.

Characterization of two diversely functionalized graphene surfaces (I versus II).
Representative plots of (A,C) Raman spectra and (B,D) respective Raman spectral images. Each pixel of the image represents data from a spectrum taken at the corresponding specific position on the surface of the graphene oxide. The red D and G band peak intensity ratio (ID/IG) is different for the two functionalized samples. The D band peak reflects the breathing vibration of sp^2 atoms in carbon rings and requires a defect for its activation, while the G band peak is due to the stretching vibration of sp^2 atoms in both rings and chains. A higher intensity ratio (ID/IG) is attributed to the formation of a covalent chemical bond between the functionalization molecule and basal planes of GO resulting in smaller sized sp^2 domains. Such influence of graphene functionalization on electrochemical performance was in agreement with other published works, as shown by (E) GO functionalized with NH_2. (F) GO functionalized with cysteamine. Reprinted, with permission, (E) from Ref. (Maity et al., 2016) (F) from Ref. (Zhou et al., 2012).

Fig. 3

Importance of cleaning bare glassy carbon electrode (GCE) and screen-printed carbon electrode (SPCE).
Cyclic voltammogram (CV) curves of (A) GCE and (B) SPCE before and after cleaning in 0.8M H_2SO_4 and 0.1M HCl aqueous mixture. CV measurements were performed in 0.1M KCl solution containing 1mM $K_3[Fe(CN)_6]/K_4[Fe(CN)_6]$. The peak-to-peak separation (ΔE) decreases and the peak currents increase after cleaning, indicating a faster electron transfer. (C) Similar results have been reported in basic solution on SPCE: CV curves (a) before, (b) after cleaning in NaOH solution by soaking 1h and (c) after anodization at 1.2V for 20s. Reprinted, with permission, (C) from Ref. (Wei et al., 2007).

Fig. 4

Electrochemical reduction of graphene oxide (GO). (A) Cyclic voltammogram (CV) curves (10 cycles, scan rate 0.1 V s^{-1}) showing the reduction of GO on SPCE in 0.1M phosphate buffer (pH 7). (B) CV curves of glassy carbon electrode (GCE), graphene oxide (GO)/GCE and reduced graphene oxide (rGO)/GCE in 0.1M KCl solution containing 1mM $K_3[Fe(CN)_6]/K_4[Fe(CN)_6]$. (C) Raman spectra plots of GO and rGO on SPCE showing an increase of I(D)/I(G) ratio after reduction. (D) X-ray Photoelectron Spectra (XPS) spectral plots of GO and rGO on SPCE showing an increase of C/O atomic ratio after reduction (C/O for GO was 2, and for rGO was 3.9). Our results were consistent with similar published studies. (E) Cyclic voltammogram curves (30 cycles, scan rate 0.03V/s) showing the reduction of GO on GCE in a solution containing 0.5 mg/ml GO with 0.05M PBS (PH 5). (F) CV curves of bare SPCE (curve a), AuNPs-modified SPCE (curve b), rGO-modified SPCE (curve c) and AuNPs/rGO modified SPCE (curve d) in 0.1M KCl solution containing 1mM $[Fe(CN)_6]^{3-/4-}$ (1:1) solution. (G) Raman spectra of graphene electrode, GO modified electrode and rGO modified electrode showing an increase of I(D)/I(G) ratio after reduction. (H) XPS spectral plots of GO and rGO modified graphene electrode showing an increase of the C/O atomic ratio after reduction. Reprinted, with permission, (E) from Ref (Devadas et al., 2012); (F) from Ref (Chan et al., 2016); (G,H) from Ref (Li et al., 2015).

Fig. 5

Electrochemical response of GO and reduced GO (rGO) modified glassy carbon electrode (GCE) with ssDNA. (A) Cyclic voltammogram curves and (B) electrochemical impedance spectroscopy (EIS) diagram showing the Nyquist plots obtained for GO (0.3mg/ml) modified GCE upon drop casting different concentrations of DNA probe recorded in 0.1 M KCl solution containing 1mM K_3[Fe(CN)6]/K4[Fe(CN)6]. Decrease of CV signal and increase of charge transfer resistance (semicycle in Nyquist plots) was attributed to the repellence of [Fe(CN)6]3-/4- ions with the negatively charged DNA molecules. (C,D) Similar trends were reported using rGO for a covalent immobilization of the DNA probe using EDC/NHS protocols before and after removal of non specific DNA absorption by keeping the electrode in the solution Tween 20. The hybridization of the DNA probe with the complementary DNA (dsDNA) further increase the negative charge on the electrode

responsible for the repellence of the redox species. (E) By increasing the complementary DNA concentration, the currents significantly decreased and (F) charge transfer resistance increases indicating more sites of the surface were occupied by DNA molecules. Reprinted, with permission, (C,D,E,F) modified from Ref. (Benvidi et al., 2015).

Fig. 6
Chart overview of Cell Therapy and Nanotechnology concepts influencing graphene Biosensor Design. Key activities and Milestones for Preclinical, Clinical and Industrial phases of development are indicated. Abbreviation: ICT (Information and communication technologies).

Table 1.
Graphene-based biosensors performance for detection of several biomarkers

Biosensor type	Detection method	Graphene-based detection platform	Analyte	Detection mechanism	Linear range	Linear regression equation / Sensitivity	Detection limit	Selectivity test real samples; interferents	Refe es
Electrochemical	SWV	HRP-$p53^{392}$Ab2-GO / phospho-$p53^{392}$ / Ab1 / NHS / AuNPs-SPCE	phospho-$p53^{392}$	sandwich type amplification strategy; GO as a nanocarrier for a high ratio of HRP / $p53^{392}$Ab2 coimmobilization	0.02 – 2 nM	-	0.01 nM	human plasma samples; interferents: p53, phospho-$p53^{15}$, phospho-$p53^{46}$	(Du al., 201
Electrochemical	DPV	Ab2 / Ag / BSA / Ab1 / chitosan-RGO / thionine / GCE	VEGFR2	sandwich type amplification strategy; improved electron transfer due to RGO excellent electrical conductivity	0.4 – 86 pM	I (μA) = 5.946 + 3.446 logC(pM)	0.28 pM	cell lysate; interferents: BSA, recombinant human $VEGF_{165}$, $VEGF_{121}$, VEGFR1 and VEGFR3	(We al., 201
Electrochemical	DPV	miRNA-H2 / MCH / BSA / H1 / AuNPs /WO3-RGO / GCE	miRNA	catalyzed hairpin assembly target recycling and enzyme signal amplificati	0.0001 – 100 pM	I(μA) = –4.98 logC(M) – 81.17	0.05 fM	human serum samples from breast cancer patients; interferents: non-	(Shu al., 201

				on; large quantity of capture probe immobilization and high electron transfer due to AuNPs/WO3-RGO hybrid				complementary, three-base mismatch, one-base mismatch sequences	
Electrochemical	EIS	ssDNA/RGO/GCE	Amylogenin DNA	hybridization of ssDNA probe with target DNA monitored by charge transfer resistance in EIS; RGO provided large surface area for DNA immobilization	2 domains: 10^{-20} – 10^{-14} M and 10^{-13} – 10^{-6} M	R_{ct} (Ω) = 0.0686 logC(M) + 2.0096 and R_{ct} (Ω) = 0.022log C(M) + 1.305	$7.1 \cdot 10^{-21}$ M	genomic DNA samples (AMGY) extracted from blood	(Ber et al 201
Electrochemical	DPV; EIS	Anti-miR-122 / Graphene/PGE	miRNA-122	Hybridization detection by guanine oxidation signal in DPV and the charge transfer resistance in EIS	0.5 – 7 μg mL^{-1}	R_{ct} (Ω) = 72574 logC(μg mL^{-1}) + 25081	1.06 pM	total RNA isolated from HUH-7 (hepatocellular carcinoma) and MCF-7 (breast cancer) cell lysates	(Kil al., 201
Electrochemical	EIS	ssDNA / GA–TRA–RGO / GCE	21-mer oligonucleotide from HBV	Hybridization reaction of ssDNA probe with target DNA monitored by charge transfer resistance in EIS	10-12 – 10-7 M	Rct (Ω) = 91.2log C(M) + 1168.5	5.2·10-13 M	non-complementary DNA sequence, one-base mismatch sequence	(Zha et al 201
Electrochemical	EIS	AAB functionalized RGO–NiO	LDL	Target analyte capturing	up to 130 mg/d	510 Ω (mg/dL)-1 cm-2	0.07 mg/dL)	real serum samples;	(Ali al., 201

		nanocomposite		by the specific probe monitored by charge transfer resistance in EIS	L			interferents: free cholesterol, total cholesterol and triglyceride	
Electrochemical	EIS	NH2-conjugated miRNAs/Carboxyl functionalized graphene	mi-RNA	Hybridization reaction of mi-RNA probe with complementary target mi-RNA monitored by charge transfer resistance in EIS	0.1pM to 1 nM	ΔRct (Ω) = 90.89+6.04 log10 (Concentration [M])	8.64· 10-14 M	single-base mismatched miRNA sequence	(Sec al., 201
Electrochemical	Amperometry	HRP - GQDs /NH2-DNA / tDNA / cDNA / Au	miRNA-155	Enzyme catalytic amplification using GQDs as platform for enzyme immobilization	1 fM – 100 pM	I (μA) = –0.8755 – 0.1083 logC(pM)	0.14 fM	miRNA-21 and completely non-complementary DNA	(Hu al., 201
FET	Electric field	VG labeled with AuNP – antibody conjugates	IgG	change in the carrier density due to the electric field gating effect; enhanced sensor stability due to vertical structure of graphene	-	-	2 ng/ml or 13 pM	IgM, HRP	(Ma al., 201
FET	Electric field	ssDNA/AuNP-CVD Graphene	DNA	electronic-doping (n-doping) introduced by hybridization with target DNAs	0.01 – 500 nM	-	0.01 nM	one-base mismatched DNA molecule	(Do al., 201
FET	Electric field	PNA/RGO	DNA	Hybridization event between PNA and	10 fM – 1 nM	-	100 fM	one-base mismatched and non-	(Cai al., 201

				DNA causes n-doping of the device due to nonelectrostatic interaction between graphene and nucleotides				complementary DNA	
FET	Electric field	Antibody probe/AuNP/Al2O3/RGO	EGP	Target EGP analyte capturing by the specific probe monitored by decrease in the electrical conductance of the RGO	-	-	1 ng/mL	Avidin and Sudan virus (SUDV) GP and Marburg virus (MARV) GP	(Ch al., 201
FET	gate capacitance shift	anti-Zika NS1 mouse mAb 6B1/CVD graphene	ZIKV NS1 recombinant antigen		-	-	0.45 nM.	Japanese encephalitis (JEV) NS1 recombinant viral antigen	(Afsahi et al., 2018)
FRET	Fluorescence intensity	fluorescein-based dye-labeled aptamer-GO	Human thrombin	FRET between GO and the aptamer modified with fluorescence groups	5 – 100 nM	-	2.0 nM	HSA, BSA, human IgG, and bovine thrombin	(Lu et al., 2009)
FRET	Fluorescence intensity	LbL-GO array	Thrombin, multiplex protein (thrombin, PDGF, VEGF, nucleolin)	FRET between GO and different target-bound aptamers labeled with dye	0.001 – 20 nM	-	0.001 nM (for 10 bilayers GO array)	BSA, STA, glucose, and IgG antibody	(Jung et al., 2013)
FRET	Fluorescence intensity	GO	miRNA let-7a	cooperative amplification combining	0.06 – 12 pM	I = 2715.37 + 4820.75	10.8 fM	human lung cells / interferents:	(Liu et al., 2014)

				with the GO fluorescence switch-based circular exponential amplification and the multimolecules labeling of SYBR Green I		C(pM)		miRNAs let-7b, let-7c, and miR-21	
FRET	Fluorescence intensity	fluorescently labeled PNAs and GO	miRNA21	GO-based fluorometric assay combined with RCA-based miRNA amplification	1 fM – 50 pM	-	0.4 pM	total cellular RNAs prepared from cultivated lung cancer cells (A549 cells); miRNA16, miRNA31 and miRNA155	(Hong et al., 2016a)
FRET	Photoluminescence intensity	afGQDs / anti-cTnI conjugate and single layer graphene	cTnI	FRET between conjugated afGQDs and graphene	1 pg mL^{-1} – 1 ng mL^{-1}	I=6208.37 logC(ng mL^{-1}) + 2901.62	0.192 pg mL^{-1}	human blood serum; interferents: non-specific antigens (HsCAg and CA15.3 Ag)	(Bhatnagar et al., 2016)
FRET	Fluorescence intensity	dye-labeled aptamer functionalized Gr on SiO2 solid support	PSA	FRET between dye-labeled aptamer and Gr	-	-	hundreds of ng/mL	albumin	(Furukawa et al., 2016)
FRET	Fluorescence intensity	fluorophore-labeled RNA aptamer / GO	theophylline	FRET between GO and fluorophore-labeled RNA aptamer	1 – 100 µM	I = 1451.7 C(µM) + 127222.5	0.155 µM	diluted urine and whole blood samples; interferents: cafeine and	(Ling et al., 2016)

								theobromine	
FRET	Fluorescence intensity	fluorophore-labeled ssDNA/GQDs	Complementary ssDNA	FRET between GQDs and fluorophore-labeled DNA aptamer	0.004–4 nM.	-	0.004 nM	-	(Yew et al., 2017)

Abbreviations:
AAB (anti-apolipoprotein B 100); Ab (antibody); afGQDs (amine functionalized graphene quantum dots); anti-cTnI (anti-cardiac Troponin I antibody); BSA (bovine serum albumin); cTnI (cardiac marker antigen Troponin I); DPV (differential pulse voltammetry); EIS (electrochemical impedance spectroscopy); FET (field effect transistor); FRET (fluorescence resonance energy transfer); GA (glutaraldehyde); GCE (glassy carbon electrode); GO (graphene oxide); GQDs (graphene quantum dots); Gr (graphene produced by chemical vapour deposition); H1, H2 (hairpin DNA); HBV (hepatitis B virus); HRP (horseradish peroxidase); HSA (human serum albumin), STA (Streptavidin); IgG (immunoglobulin G); IgM (immunoglobulin M); LbL (layer-by-layer); LDL (low density lipoprotein); MCH (diethylpyrocarbonate 6-mercaptohexanol); PGE (pencil graphite electrode); phospho-p53392 (phosphorylated p53 protein at Ser392); PNA (peptide nucleic acid); PSA (prostate specific antigen);RCA (rolling circle amplification); RGO (reduced graphene oxide); SPCE (screen printed carbon electrode); SWV (square wave voltammetry); TRA (tryptamine); VEGFR2 (vascular endothelial growth factor receptor 2); VG (vertically-oriented graphene).

Table 2
Performances of different nanomaterials-based biosensors for miRNA biomarkers detection.

Detection method	**Nanomaterial-based detection platform** / *Aptamer Affinity Probe*	Analyte	Linear range (fM)	Detection limit (fM)	References
Fluorescence	**GO** / *fluorescently labeled PNA*	miRNA21	1 – 50,000	400	Hong et al., 2016
Fluorescence	**MoS_2** / *fluorescently labeled ssDNA*	miRNA21	0 – 40,000000	50,000	Cai et al., 2018
ECL	**Fe3O4@Au MNPs-cDNA** / (*sDNA&luminol*)@**GO**	microRNA-21	1 –10,000	0.3	Lu et al., 2017
UV-vis spectrophotometry	**Positively charged AuNPs** / *DNA*	miRNA21	20,000 – 10,000000	6800	Miao et al., 2016
Electrochemical (SWV)	**MoS_2**-Thi-AuNPs /GCE	miRNA21	1000 – 10,000000	260	Zhu et al., 2017
Electrochemical (DPV)	**Au** / **SWCNTs / NDs** / **SWCNTs** / **AuNPs** / *TSP-cDNA* / **AuNPs-hemin-G-quadruplex**	miRNA21	10 – 1000	1.95	Liu et al., 2015b

Electrochemical (DPV)	**GO** / **GNR** / *OB*	miRNA-155	2 – 8000	0.6	Azimzadeh et al., 2016
Electrochemical (Amperometry)	**Au** / *cDNA* / *tDNA* / *NH2*-**GQDs-HRP** / *DNA*	miRNA-155	1 – 100,000	0.14	Hu et al., 2016
Electrochemical (DPV)	**GO** / **AuNP** / *SH-DNA* / *SH-CPs, HCR-CHA* / *MB*	miRNA-155	10 – 1,000000	3.3	Wu et al., 2014
Electrochemical (CV)	**NF** / *Thi* / PdNPs	miRNA-155	5,600 – 5.6×10^{8}	1870	Wu et al., 2013
Electrochemical (SWV)	*ssDNAPbS+ssDNACdS* (**QDs**)/ssDNA-MB	miRNA-155	50 – 30,000	12	Zhu et al., 2014
FET	**MoS_2**	miRNA-155	0.1 – 10,000000	0.03	Majd et al., 2018
FET	**rGO-AuNPs** / *PNA*	miRNA let-7b	1 – 100,000	10	Cai et al., 2015

Abbreviations:
AuNPs (gold nanoparticles); *cDNA* (target DNA); *CHA* (catalyzed hairpin assembly reaction); CV (cyclic voltammetry); DPV (differential pulse voltammetry); ECL (Electrochemiluminescence); **Fe_3O_4@Au MNPs**- *cDNA* (magnetite@gold magnetic nanoparticles-capture DNA); FET (field effect transistor); **GNRs** (gold nanorods); **GO** (graphene oxide); **GQDs** (graphene quantum dots); *HCPs* (hairpin-shaped capture probes); *HCR* (hybridization chain reaction); *MB* (methylene blue); **MoS_2** (molybdenum disulfide)**ND**s (nanodiamonds); *NF* (nafion); *OB* (Oracet Blue); **PdNPs** (palladium nanoparticles); *PNA* (peptide nucleic acid); **RGO** (reduced graphene oxide); *SH-CPs* (Thiolated helper capture probe); *SH-DNA* (Thiolated helper DNA probe); *ssDNA***PbS**+*ssDNA***CdS** (**QD**s) (affinity probes labeled with single stranded DNA lead sulfide and cadmium sulfide quantum dots) **SWCNTs-ox** (oxidized single-walled carbon nanotubes); SWV (square wave voltammetry); *Thi* (thionine); *TSPs* (tetrahedron-structured probes); (*sDNA*&l*uminol*)@**GO** (signal unit GO labeled by luminol and signal DNA);

Highlights

- Cell based gene therapy against cancer and stem cell therapy for tissue regeneration have recently achieved clinical approval.
- Novel graphene based biosensors can detect biomarkers relevant to human cell therapy.
- We highlight biomarker significance and biosensor applications in the context of cancer and stem cell assays.
- The versatility of graphene based modifications complements the diverse nature of cellular assays.
- Concepts and parameters influencing graphene based biosensor design for cell therapy are critically reviewed.

Figure 1.

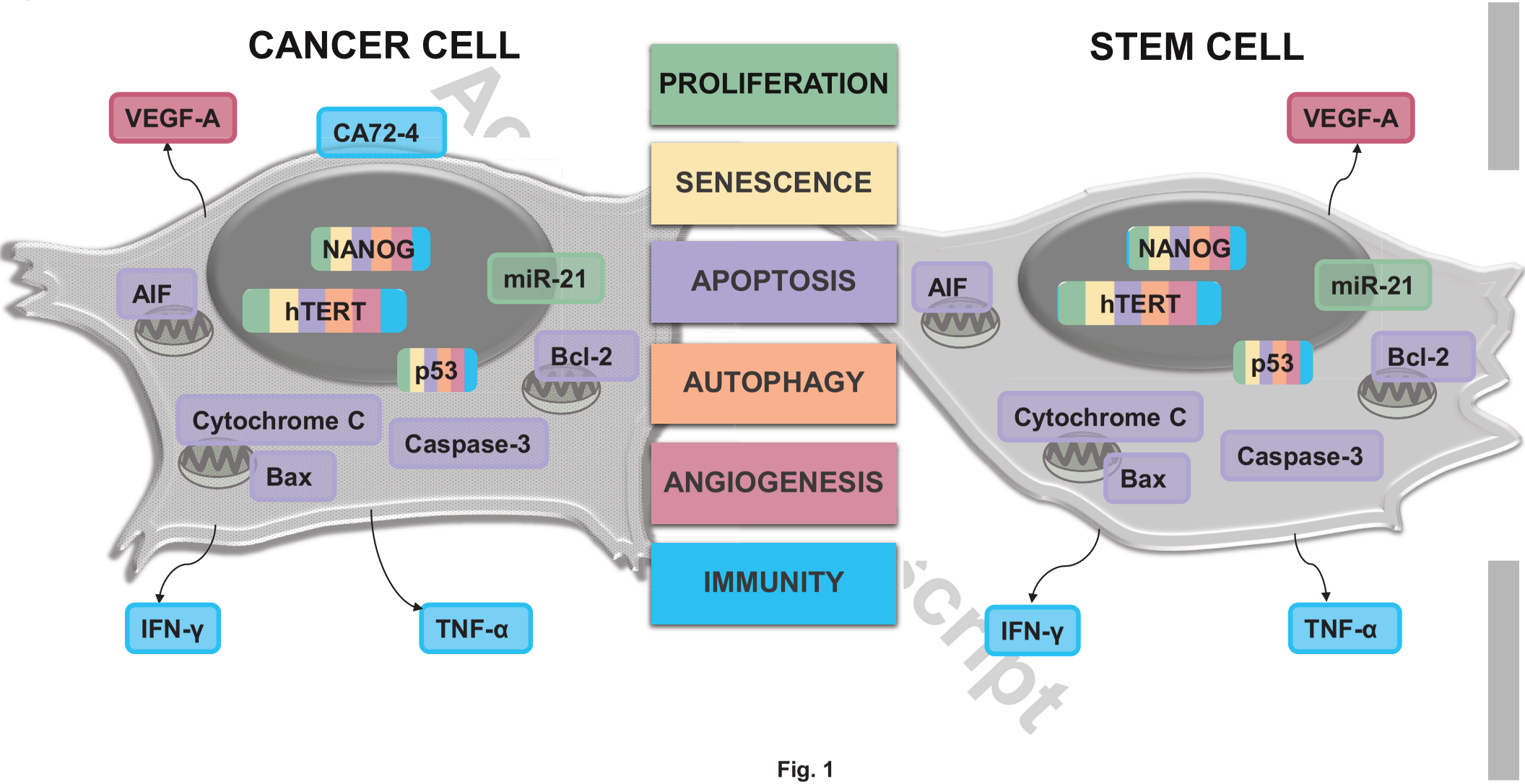

Fig. 1

Figure 2

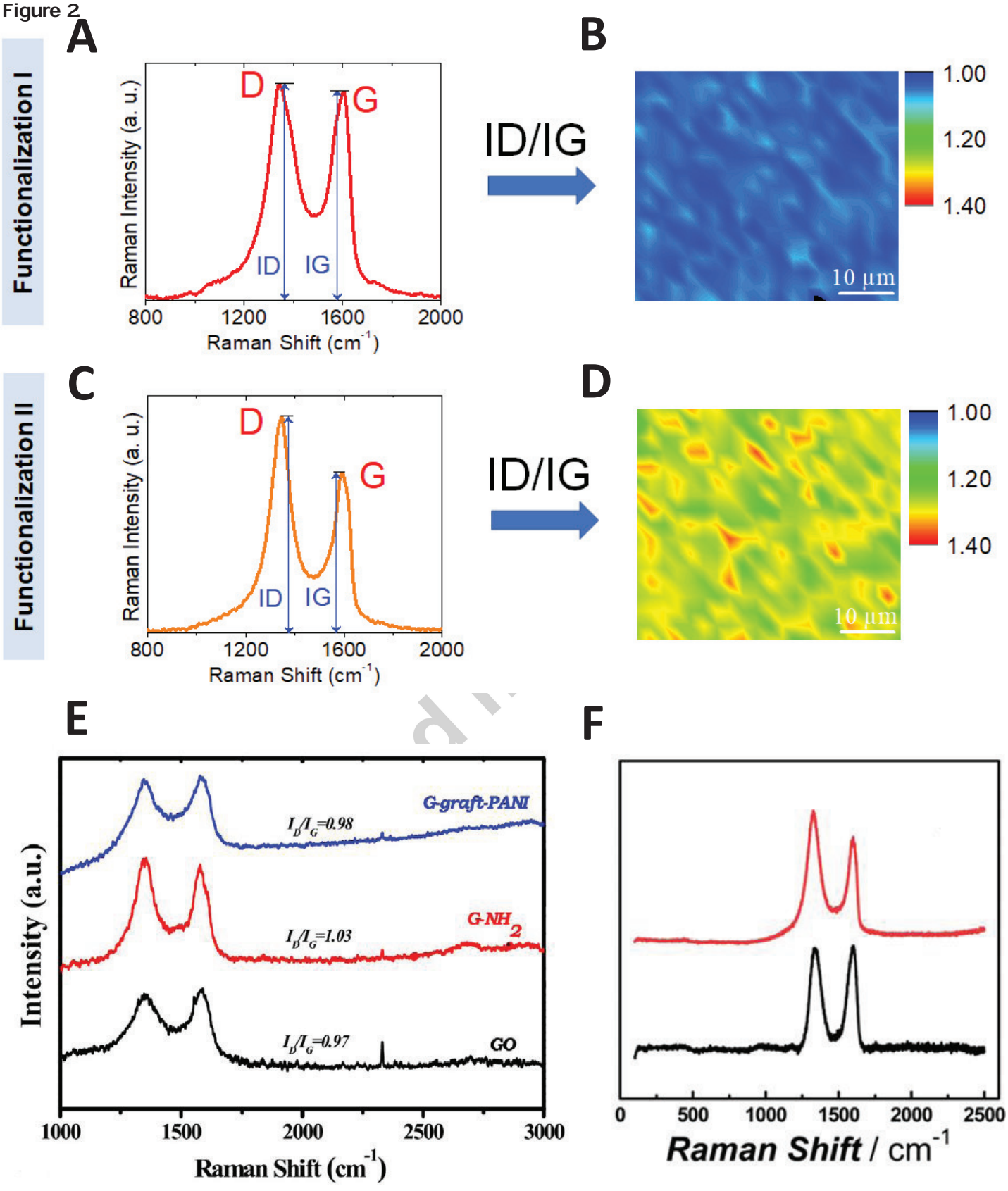
A
B
Functionalization I
D
G
ID
IG
Raman Intensity (a. u.)
800
1200
1600
2000
Raman Shift (cm-1)
ID/IG
1.00
1.20
1.40
10 μm
C
D
Functionalization II
E
F
G-graft-PANI
ID/ID=0.98
G-NH2
ID/IG=1.03
GO
ID/IG=0.97
Intensity (a.u.)
1000
1500
2000
2500
3000
Raman Shift (cm-1)
0
500
1000
1500
2000
2500
Raman Shift / cm-1

Figure 3

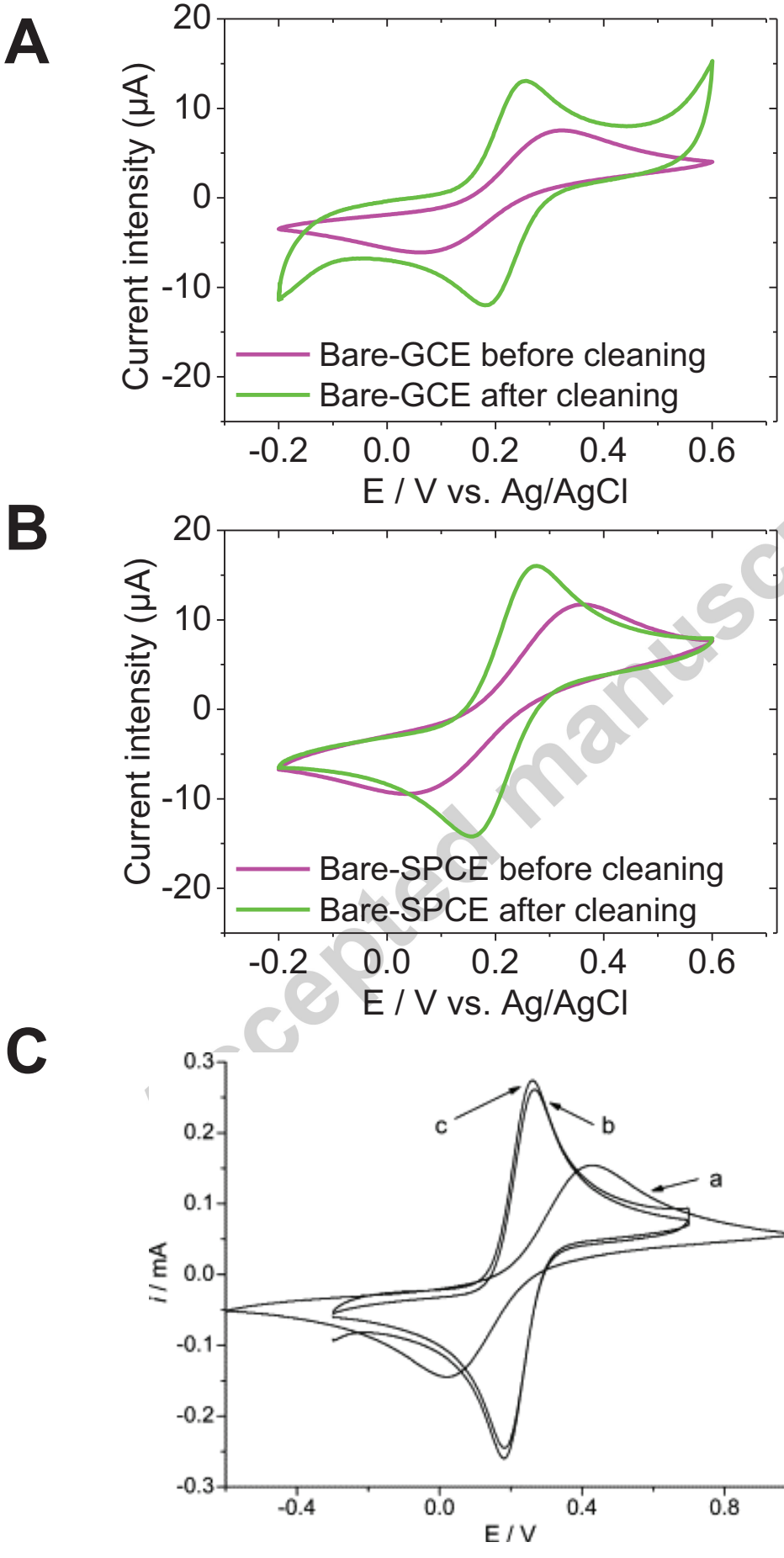

Figure 4

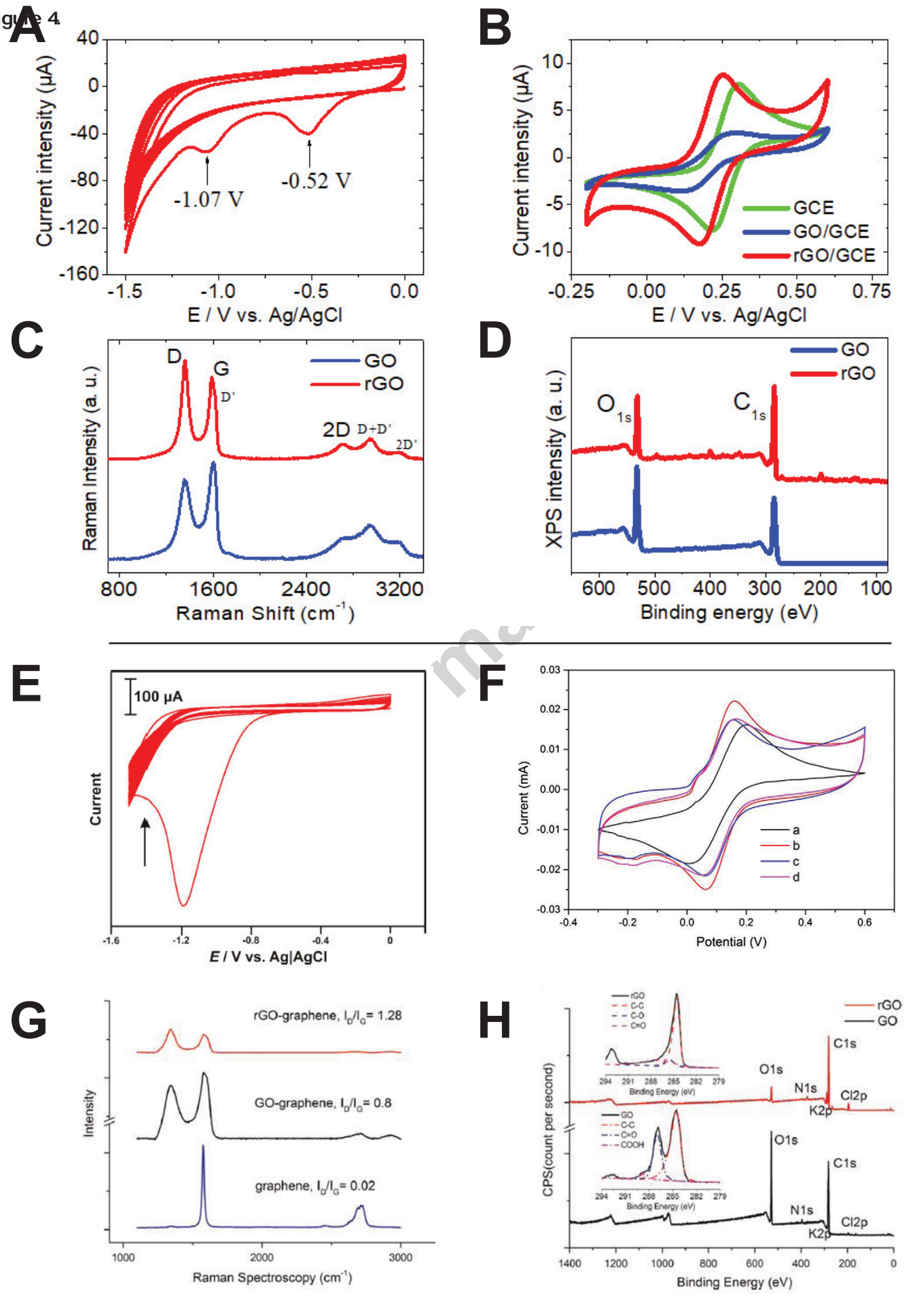

Figure 5

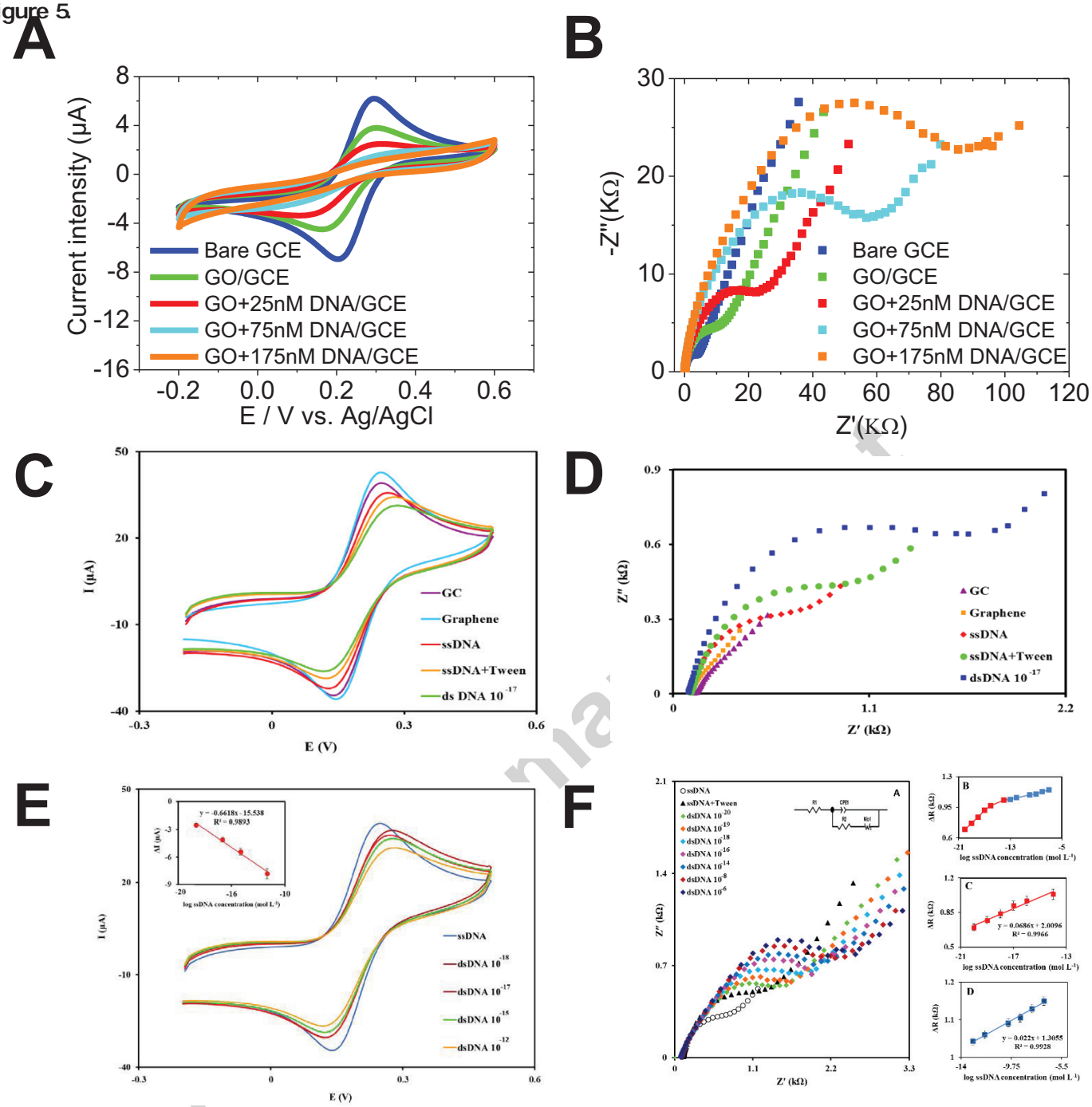
A
Current intensity (μA)
E / V vs. Ag/AgCl
Bare GCE
GO/GCE
GO+25nM DNA/GCE
GO+75nM DNA/GCE
GO+175nM DNA/GCE
B
-Z''(KΩ)
Z'(KΩ)
Bare GCE
GO/GCE
GO+25nM DNA/GCE
GO+75nM DNA/GCE
GO+175nM DNA/GCE
C
I (μA)
E (V)
GC
Graphene
ssDNA
ssDNA+Tween
ds DNA 10 -17
D
Z'' (kΩ)
Z' (kΩ)
GC
Graphene
ssDNA
ssDNA+Tween
dsDNA 10 -17
E
I (μA)
E (V)
y = -0.6618x - 15.538
R² = 0.9893
log ssDNA concentration (mol L-1)
ssDNA
dsDNA 10 -18
dsDNA 10 -17
dsDNA 10 -15
dsDNA 10 -12
F
ssDNA
ssDNA+Tween
dsDNA 10 -20
dsDNA 10 -19
dsDNA 10 -18
dsDNA 10 -16
dsDNA 10 -14
dsDNA 10 -8
dsDNA 10 -6
Z'' (kΩ)
Z' (kΩ)
A
B
C
y = 0.0686x + 2.0096
R² = 0.9966
D
y = 0.022x + 1.3055
R² = 0.9928
log ssDNA concentration (mol L-1)